Article

Grease, Oxygen, and Air Barrier Properties of Cellulose-Coated Copy Paper

Ronald Sabo [1,*], Cody Schilling [1], Craig Clemons [1], Daniel Franke [1], Neil R. Gribbins [1], Michael Landry [2], Kimberly Hoxie [1] and Peter Kitin [1]

1   USDA Forest Service Forest Products Laboratory, Madison, WI 53726, USA; cody.schilling@usda.gov (C.S.); craig.m.clemons@usda.gov (C.C.); daniel.franke@usda.gov (D.F.); neil.r.gribbins@usda.gov (N.R.G.); kimberly.l.hoxie@usda.gov (K.H.); peter.kitin@usda.gov (P.K.)
2   Biological Systems Engineering, University of Wisconsin, Madison, WI 53706, USA; michaellandry5666@gmail.com
*   Correspondence: ronald.sabo@usda.gov

Abstract: Cellulose nanomaterials have been demonstrated to be excellent barriers against grease, oxygen, and other vapors, but their implementation in packaging materials is challenging because of numerous technical and practical challenges. In this work, the oxygen, air, grease, and heptane barrier performance of copy papers coated with cellulose nanocrystals (CNCs), oxidized cellulose nanofibrils (TOCNs), and carboxymethyl cellulose (CMC) weas examined. The effects of different materials and processing conditions were evaluated for their impacts on the resulting barrier properties. TOCN coatings demonstrated significantly better barrier properties than CNC and CMC coatings due to the long-range networked structure of TOCN suspensions eliciting enhanced film formation at the paper surface. Neat coatings of nanocellulose did not readily result in strong oxygen barriers, but the addition of CMC and/or an additional waterborne water barrier coating was found to result in oxygen barriers suitable for packaging applications (1 cm^3/m^2·day transmission at low humidity with a 10 g/m^2 coating). Cast films and thick coatings of CMC were good barriers to oxygen, grease, and air, and its addition to cellulose nanomaterial suspensions aided the coating process and reduced coating defects. In all cases, the incorporation of additional processing aids or coatings was necessary to achieve suitable barrier properties. However, maintaining the strong barrier properties of nanocellulose coatings after creasing remains challenging.

Keywords: cellulose nanofibrils; cellulose nanocrystals; carboxymethyl cellulose; barrier coatings; air permeability; grease resistance; oxygen transmission; packaging applications

1. Introduction

The need for environmentally friendly packaging materials is growing rapidly. It is estimated that packaging contributes to roughly 47% of the 8–11 million tons of synthetic plastics that end up in the oceans each year [1]. Wood-derived materials are of great interest because of their biodegradability and sustainability. Cellulose nanomaterials (CNMs) have been shown to have good barrier properties against grease, oxygen, and other gases [2–6]. The barrier properties of cellulose nanomaterials in the form of cast films [7–11], coated polymer films [12–16], laminates [17–19], and coated paper substrates [20–24] have been measured. Fukuzumi et al. coated polymer films with TEMPO ((2,2,6,6-Tetramethylpiperidin-1-yl)oxyl)-oxidized cellulose nanofibrils (TOCNs) to create coatings that were 0.4–1.5 μm thick and found significantly reduced oxygen transmission compared to uncoated polymer films [25,26]. At 0% relative humidity (RH), the oxygen transmission rate (OTR) of PLA was reduced by four orders of magnitude by coating it with 1.5 μm of TOCNs, but the OTR improvements at 75% RH were small [26]. Koppolu et al. investigated the use of CNCs and MFC as barrier coatings on paperboard, and they also laminated the paperboard with PLA films [20,21]. They found that CNCs could reduce

the OTR by 98% at 50% RH, although there was little improvement in the OTR at 90% RH compared to PLA controls [21]. Nanocellulose-coated papers were also found to be good grease barriers [27–31]. For example, Tayeb et al. found that lignin-containing cellulose nanofibrils (CNFs) coated on paper had excellent grease resistance with a kit rating of 12, and bowls shaped from the coated paper were able to hold grease for months [30]. However, much is still not understood about the effects of formulation and processing on the barrier performance of paper-based substrates coated with cellulose nanomaterials. Furthermore, there is a need to explore the use of water barriers and/or additives to improve the performance of nanocellulose-based coatings.

Although improved barrier properties of papers coated with nanocellulose have been demonstrated, the effects of the nanocellulose type and the processing conditions are not well understood. Polymers, cross-linking agents, and other chemicals have also been added to nanocellulose for paper coatings, but the roles or impacts of these additives are not always clear. Koppolu et al. evaluated both microfibrillated cellulose (MFC) and CNCs as barrier coatings on paperboard, and the performance between the materials appeared to be similar, although the MFC coatings generally had lower OTR values at an elevated humidity compared to the CNC coatings [21]. Gicquel et al. found that adding polyethylene glycol (PEG) to a CNC coating on paper improved its grease resistance, but they also noted that the results were not as favorable as some in the literature obtained using CNFs [32]. Koppolu et al. found that adding sorbitol to CNCs resulted in a less brittle paperboard coating, and that the performance, especially the water vapor transmission rate (WVTR), of CNC coatings with sorbitol was somewhat improved [20]. Herrera also found that filter paper dip-coated with CNCs that were plasticized with sorbitol had a lower oxygen permeability than filter paper coated with CNCs without sorbitol, but sorbitol was not observed to improve the water vapor transmission results [33]. Herrera et al. used citric acid for the cross-linking of CNC coatings on filter paper, but few properties appeared to be improved with the addition of citric acid [33]. Du et al. added borate modified polyvinyl alcohol (PVOH) to sulfonated nanofibrillated cellulose and chitosan, and found the samples with modified PVOH had the maximum grease resistance rating [22]. It is not clear from that work what the impact of nanocellulose is on the coating performance. Therefore, additional evaluations of nanocellulose types, processing conditions, and formulations on paper barrier coatings are warranted and are carried out in this work.

Carboxymethyl cellulose (CMC) is a water-soluble polymer that is mostly produced from plants and that is used in food, pharmaceutical, and many other applications [34], including as a component of cellulose nanomaterial coatings on paper [20,24,35]. Koppolu et al. evaluated CMC as one of several base layers for the CNC coating of paper, and found that CMC had extremely low air permeability [20]. Basta et al. effectively used CMC as a base layer for coating paper with chitosan, significantly reducing the water vapor permeability [35]. However, the impact and role of CMC beyond functioning as a base coating was not clear. He et al. coated filter paper using CMC with and without CNCs/silver nanoparticles (CNC-AgNP), and found that all coated papers, especially those with higher CNC-AgNP contents, had reduced air permeability, increased tensile strength, and slightly reduced water permeability compared to the uncoated paper [24]. However, they did not evaluate CNC coatings without CMC, so the impact of CMC on the coatings is not clear. Evaluation of the properties of CMC with and without cellulose nanomaterials is an objective of the current work.

Achieving coating durability is another challenge for the practical application of cellulose nanomaterial-based barrier coatings. These coatings are generally brittle and exhibit failures when stressed or deformed, but limited evaluations of their durability have been performed [11,27,30,36,37]. Chen et al. showed that adding sorbitol to CNCs led to films that were more flexible than those without CNCs, but the barrier properties of folded or creased samples were not evaluated [38]. Li et al. used a flex tester to evaluate the durability of CNC coatings on polymer films and found that the oxygen permeance deteriorated after the films were flexed [36]. Researchers at the University of Maine have

evaluated the effect of folding on CNF films and coated papers by applying weight to the folded paper for a fixed time (5 kg for 5 min [37]; 1 kg for 2 min [27]; 2.5 kg for 10 min [11]). Tayeb et al. found that lignin-containing CNFs had more resistance to breaking after folding than CNFs from bleached pulp, and that a grease kit rating of 12 was maintained even in a 180° folding event [30]. Hasan et al. showed that films of mechanically produced CNFs maintained their low oxygen transmission with a single fold but not with two crossing folds [11]. More investigations are needed to determine how the barrier properties of papers coated with various types of CNMs are affected by folds, creases, and other defects.

This work is motivated in part by the lack of understanding of the impact of material formulations, water barrier coatings, and processing on the barrier properties of coated paper. Here, the grease, air, and oxygen barrier properties of papers coated with different cellulose-based coatings are measured under various processing conditions, including varied coating speeds and variation in whether the nanomaterials were sonicated. The barrier properties of CNCs, TOCNs, and CMC are compared, and the effects of adding CMC to CNCs and TOCNs are evaluated. The processing effects of different suspension preparations and coating conditions are examined, including the resulting morphological, rheological, and barrier properties resulting from sonicating TOCNs. The effects of creasing coated papers on their barrier properties, including their oxygen transmission and grease penetration, are examined. Furthermore, the effect of adding a water barrier layer on top of cellulose nanomaterial coatings is explored.

2. Materials and Methods

2.1. Materials

Two types of copy paper were used for this study. Skilcraft® NATURE-CYCLE 100% post-consumer fiber copy paper (Shreveport, LA, USA) was denoted as Copy1 and Boise® ASPEN® 30 Multi-Use Recycled Copy Paper (Boise Paper, Packaging Corporation of America, International Falls, MN, USA) was denoted as Copy2. Unless specified otherwise, Copy1 was used. Silicone-coated release paper was obtained from Griff and Associates (Levittown, PA, USA). Reynolds® Genuine Parchment Paper was used (Reynolds Consumer Products Inc., Richmond, VA, USA). Canola oil (The Kroger Co., Cincinnati, OH, USA), n-heptane (EMPLURA® brand purchased from Sigma-Aldrich St. Louis, MO, USA), and castor oil (Horbäach brand) were all used for barrier testing. Carboxymethyl cellulose (CMC) with a molecular weight of 250,000 and 0.9 degrees of substitution was purchased from Sigma-Aldrich (St. Louis, MO, USA). Reagent grade toluene was purchased from Thermo Fisher Scientific (Waltham, MA, USA). Melodea VBCoat® was the water barrier layer used for this work and was kindly supplied by Melodea Ltd. (Rehovot, Israel). Apiezon type "T" vacuum grease was obtained from AMETEK MOCON (Brooklyn Park, MN, USA) and Structure Probe, Inc. (West Chester, PA, USA). Solutions of starch (PENFORD® GUM 280, Ingredion Inc., Westchester, IL, USA) were prepared by adding powdered starch to deionized water at approximately 15% solids content by weight, followed by heating just below 100 °C while stirring for approximately 30 min. Cupriethylenediamine, 1.0 M, was purchased from Ricca Chemical (Arlington, TX, USA).

2.2. Suspension Preparation

All cellulose nanomaterials were produced in the USDA Forest Service, Forest Products Laboratory pilot plant facility. Suspensions of ~10 wt.% cellulose nanocrystals (CNCs) were produced from dried dissolving pulp as described previously [39]. Suspensions of 1 wt.% TOCNs were produced from bleached Kraft pulp under alkaline conditions as described elsewhere [40,41]. Suspensions of CNCs and TOCNs were also prepared with CMC. CMC was added to CNC or TOCN suspensions at a ratio of 100:20 or 100:10 nanocellulose to CMC on a dry weight basis. Water was added to CNC suspensions to give solid contents of approximately 6% by weight unless otherwise noted. The suspensions were placed in a water bath at 60 °C and stirred with an impeller for approximately one hour. TOCN suspensions were then degassed under vacuum until no bubbles were visible. Some samples

were sonicated, as indicated, using a Fisher Scientific model FB705 Sonic Dismembrator (Thermo Fisher Scientific, Waltham, MA, USA) at 50% power. Aqueous CMC solutions (5–7% solids contents) were also prepared in a similar manner, as a useful comparison.

2.3. Paper Coating and Film Casting

Copy paper was coated using a compact tape casting film coater (MSK-AFA-III) manufactured by MTI Corporation (Richmond, CA, USA). Papers were first cut to approximately 18 cm wide by 33 cm long and were then taped along the edges to the vacuum plate of the coater. For some CNC coatings, hand soap was applied to the vacuum plate on the coater to prevent sticking of the paper to the plate. Vacuum was applied to hold the paper in place and to minimize distortion during the coating and drying process. Vacuum levels were generally kept between −10 and −40 kPa. Coatings were applied by a 10 cm wide doctor blade translated along the length of the paper. The gap between the paper and doctor blade was adjusted to control coating thickness. After coating, the top of the apparatus was closed, and coatings were dried by forced air from above the paper. The setpoint for the forced air was 35 °C unless otherwise specified. Coating weights were determined gravimetrically, and a linear least squares regression estimate was used to calculate an estimated weight for each doctor blade gap setting. Creased specimens were prepared according to TAPPI T 512-07, in which each 100 mm squared paper specimen is folded diagonally and pressed with a 2.04 kg creasing roller, then folded in the opposite direction and rolled again. Films were cast in 100 mm diameter polystyrene petri dishes by evaporative drying at room temperature. The thickness of cast films was typically between 50 μm and 120 μm.

2.4. Grease Penetration Testing

Grease penetration was determined by measuring the amount of dyed canola oil that flowed through the paper and was transferred to a clean blotter paper, in accordance with TAPPI T 507 [42]. A stack of up to 10 specimens was measured at once. A rigid metal plate was used as a base for the stack. Each test specimen consisted of a 100 mm squared of aluminum foil on the bottom, a 100 mm square of white blotter paper (smooth side up), a 100 mm squared of coated paper (coated side up), a 75 mm squared of white blotter paper soaked in red dyed oil, and another 100 mm squared of aluminum foil on the top. After stacking up to 10 specimens, a 400 g, 100 mm squared block was placed on top of the stack. The assembly was placed in an oven for 4 h at 60 °C. The 100 mm squared receiving blotter paper specimens were placed on a drying rack for approximately 24 h before we performed image analysis. The blotter paper was placed on a scanner with a green background, scanned in 24-bit color at 600 dots per inch, and saved as a TIFF file. The green image was subtracted from the scan to determine the pixel count of the total area of blotter paper, and then the pixels of red-dyed areas were counted. The ratio of red to total blotter paper area is reported as percent coverage. The dyed oil was made by combining 1 g of oil-soluble red dye with 100 mL of canola oil.

Grease resistance was also measured using TAPPI T559, commonly known as the TAPPI kit test [43]. Twelve solutions consisting of castor oil, n-heptane, and/or toluene were prepared and numbered according to the ratios specified in the standard. Solution 1 consisted only of castor oil, and solutions 11 and 12 only contained heptane and toluene, with each solution having progressively lower surface energies. The test was performed by placing a drop of solution on coated paper, waiting 15 s, wiping the drop away, and evaluating whether a stain was left. If a stain was left, the test was a failure, and a lower-numbered solution was tested. If no stain was left, the test was a pass, and a higher-number solution was tested. The kit rating was determined as the highest-numbered solution that passed the evaluation with no stain.

2.5. Heptane Transmission

Heptane vapor transmission measurements were made based on the ASTM E96 standard for measuring water vapor transmission [44]. Approximately 25 mL of n-heptane

was added to vapor transmission cups (EZ-Cup Vapometer Permeability Cup, Thwing-Albert, West Berlin, NJ, USA). Coated papers were placed in the cups between gaskets, and these were sealed by screwing the top ring onto the cup. The weight of the assembly was measured over regular intervals for up to 2 days. Heptane vapor transmission rates (HVTR) were calculated as

$$HVTR = \Delta W / \Delta t / A_c \tag{1}$$

where $\Delta W / \Delta t$ is the linear fit of the change in weight over time and A_c is the cross-sectional area of the cup openings, which was 0.003167 m^2.

2.6. Oxygen Transmission

Oxygen transmission measurements were taken on a MOCON OX 2/22L (AMETEK MOCON, Brooklyn Park, MN, USA) based on ASTM D3985 [45] at 23 °C at various levels of relative humidity. Setpoints for relative humidity were kept the same for test and carrier gas streams. Each sample run was programmed with repeating 60 min test cycles with a convergence criterion of 2% across the last three test cycles at each humidity step to ensure sample equilibrium. An instrument re-zero was performed for 60 min at the beginning of each sample run and was repeated every eight testing cycles throughout the full sample convergence run. A minimum of two replicates of all sample types were tested for oxygen permeability. Oxygen transmission rate (OTR) values generated by the instrument were then converted to permeance and permeability values as follows.

$$Permeance = OTR/(xP) \tag{2}$$

where x is the mole fraction of oxygen in the test gas (1 in this case), and P is the total pressure measured and reported by the instrument. Oxygen permeability was calculated as

$$Permeability = Permeance \times d \tag{3}$$

where d is the sample thickness. The thickness of each sample was measured at 10 locations within the oxygen permeation area using a digital thickness gauge (Checkline MTG-DX2-W, Electromatic Equipment Co. Inc., Lynbrook, NY, USA) with a 100 g mass and 3.2 mm diameter presser foot. The average of the 10 thickness measurements was used to calculate permeability.

2.7. Air Permeability

Air permeability measurements were done using two different instruments. Specimens of at least 50 mm squared were prepared for testing, and, typically, testing was done with coating side both up and down. An oil-sealed Gurley apparatus (Teledyne Gurley, Troy, NY, USA) was used for some of the testing, in accordance with TAPPI T460 [46]. The tester was equipped with an optical sensor to begin and stop the timer based on a pre-set volume of air. For uncoated specimens, the time to reach 100 mL of air displacement was measured, but for coated samples, lower volumes (12.5–50 mL) were used because of the long times required. A Technidyne PROFILE/Plus Roughness & Porosity (Industrial Physics, New Albany, IN, USA) was also used to measure air permeability. This Technidyne porosity instrument uses compressed air for permeability testing, and the tests can be done over a range of pressures corresponding to various test standards. This study used the Oil Gurley [46] method on the Technidyne instrument.

2.8. Scanning Electron Microscopy

Paper cross-sections were prepared either by freezing in liquid nitrogen followed by fracturing with a razor blade, or by embedding samples in Sylgard 184 silicone elastomer resin, which was kindly provided by Dow Inc. (Midland, MI, USA), followed by microtome cross-sectioning. The resin was prepared using a 10:1 ratio of prepolymer:curing agent. Paper samples were submerged in the resin and put under mild vacuum until the samples

were fully impregnated and the resin was degassed. The paper samples were then embedded in the resin molds and cured at 70 °C for 4 h. Cross-sectional surfaces were prepared using a rotary microtome (Model UC7, Leica, Deerfield, IL, USA). Both cross-sections and surface analysis samples were adhered to aluminum stubs using either doubled-sided copper or carbon tape and were coated with a thin layer of gold to enhance conductivity. Samples were imaged using a Zeiss Evo 15 LS SEM (Carl Zeiss Microscopy GmbH, Jena, Germany) with an accelerating voltage of 3–10 kV. Coating thicknesses were determined with ImageJ®, version 1.54g, using an average of 10 measurements made across the field of view [47].

2.9. Dynamic Light Scattering

Dynamic light scattering (DLS) analyses were conducted using a NanoBrook Omni (Brookhaven Instruments, Holtsville, NY, USA) particle size analyzer. One percent solids content suspensions of TOCNs were sonicated at 50% amplitude to total energy inputs ranging between 0 and 10 kJ/g TOCN. DLS samples were diluted to 0.01% solids content in deionized water and mechanically stirred with an impeller mixer for 30 min at 500 RPM. The suspensions were then centrifuged at 3500 RPM for 30 min. The supernatants were analyzed using the backscattering setting (173°) and the size intensity distribution of each sample was determined based on the autocorrelation functions using the CONTIN algorithm. Each replicate was reported as the average of 5 measurements, with a minimum of 3 replicates taken for each sample. Error bars for DLS data represent the standard deviation from the mean.

2.10. Degree of Polymerization

Degree of polymerization (DPv) measurements for the various ultrasonication energy inputs were taken according to the TAPPI T 230 standard [48]. Following ultrasonication, TOCN suspensions were freeze-dried (Model 73820, Labconco, Kansas City, MO, USA) and stored in a desiccator prior to analysis. Freeze-dried samples were dissolved in 0.5 M copper ethylenediamine solution for 15 min under a flow of nitrogen. The intrinsic viscosities were determined using Cannon-Fenske capillary viscometers at 25 °C, and DP_v values were calculated using the Mark–Houwink–Sakurada equation [49]:

$$[\eta] = 1.75 \times DP_v. \tag{4}$$

2.11. Rheological Measurements

Small-amplitude oscillatory shear (SAOS) tests on both sonicated (10 kJ/g) and unsonicated 1% dispersions of TOCNs were conducted using an MCR 302 strain-controlled rheometer (Anton Paar, Graz, Austria). A parallel plate geometry with a diameter of 24.5 mm was used and all measurements were performed at 25 °C. Grade P220 sandpaper (3M, Maplewood, MI, USA) was glued with epoxy to the surfaces of both plates to minimize wall slip and a hood was used to minimize water evaporation. Select tests were performed at multiple plate gaps to investigate wall slip or shear banding where indicated. Results using a 1 mm gap are presented in the figures and tables unless otherwise noted.

Sixty-minute time-sweeps at a strain amplitude of 0.5% and a frequency of 1 Hz were used to determine that a 10 min rest time was required for the sample to recover from the loading of the sample and its compression when the gap was set. The tests also verified that the rheological properties did not change due to water evaporation during the time of testing. Amplitude sweeps from 0.1 to 500% at 1 Hz were performed to determine the effects of amplitude on the rheological properties as well as on the yield and flow points. The yield point was taken as the point where the storage modulus was reduced by 5%. The flow point was taken as the point at which the storage and loss moduli curves crossed. Three interval thixotropy tests (3ITT) were used to investigate the recovery of the sample after shearing. The 1st and 3rd intervals were performed in oscillation at a strain amplitude of 0.5% and a frequency of 1 Hz. The 2nd interval was performed in rotation at shear rates of 67, 200, or 500 s^{-1}.

3. Results and Discussion

Applying cellulose nanomaterials as coatings is challenging for various reasons, including the large water content and high viscosity of the suspensions used, the brittleness of the coatings, the propensity of the coatings for defects, the lack of durability or creasing resistance, and the complexity of drying, residual stresses, and distortion. The amount of literature on the coating of papers with cellulose nanomaterials is relatively limited, especially considering the interest in using cellulose nanomaterials for packaging applications [2,5,50–52]. These challenges to applying nanocellulose coatings with good barrier properties are likely one of the reasons the field has not advanced more quickly. This work attempted to delineate some of the effects of processing, coating formulations, and the nanocellulose type on the barrier properties of coated copy paper.

3.1. Comparison of Neat Cellulose Coatings

3.1.1. Scanning Electron Microscopy of Neat Coatings

Electron micrographs of coated papers are shown in Figures 1 and 2. The cross-sections of the TOCN-coated papers show a layered coating on top of the paper substrate, whereas the CNC-coated papers have less pronounced coating layers, suggesting that CNCs penetrated the papers. Figure 1 depicts two coating weights for both the CNCs and TOCNs which reflect the difference in the film-forming behavior of the two CNMs. CNCs appear to fill voids in the papers, leaving fibers easily resolved, even at higher coating weights. As the TOCN coating weight was increased, continuous coating films were observed. Additionally, Figure 2A,B show the increase in paper penetration by CNCs at higher coating weights. During the coating process, CNCs would often be observed to penetrate through the paper, sometimes causing the paper to stick to the vacuum plate after drying. Note that measuring the coating weights, especially of small samples, was challenging and exhibited substantial variability within and between samples. The coating thicknesses for the papers in Figure 1B–D were estimated to be approximately 4 g/m^2, 8 g/m^2, 1 g/m^2, and 12 g/m^2, respectively, and those for Figure 2A–D were estimated to be approximately 4 g/m^2, 8 g/m^2, 2 g/m^2, and 12 g/m^2, respectively.
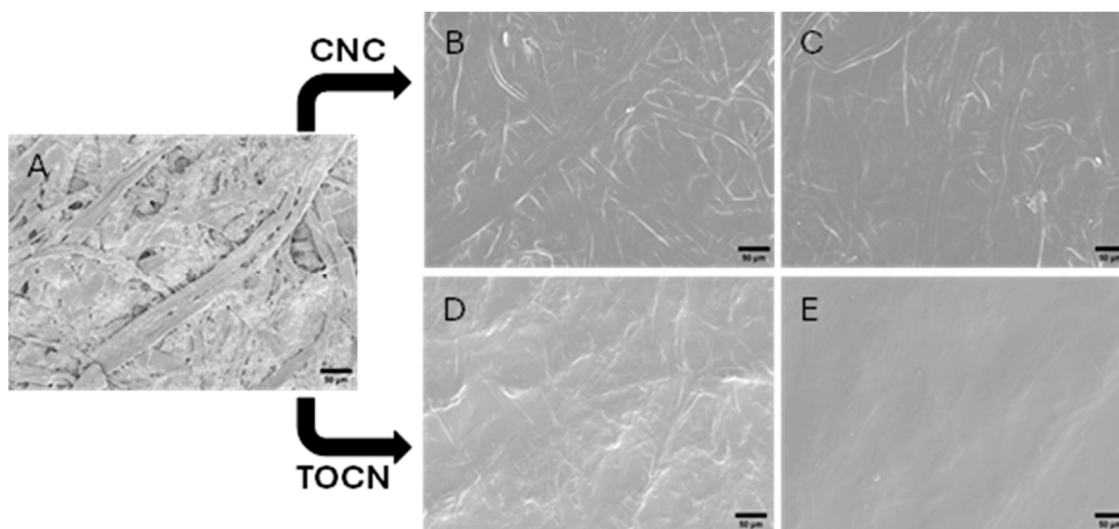

Figure 1. SEM micrographs of uncoated copy paper, and CNC- and TOCN-coated paper surfaces; (**A**) uncoated copy paper; (**B,C**) CNC coatings with doctor blade settings of 50 and 100 μm, respectively; (**D,E**) TOCN coatings with doctor blade settings of 150 and 2000 μm, respectively. Scale bars represent 50 μm.
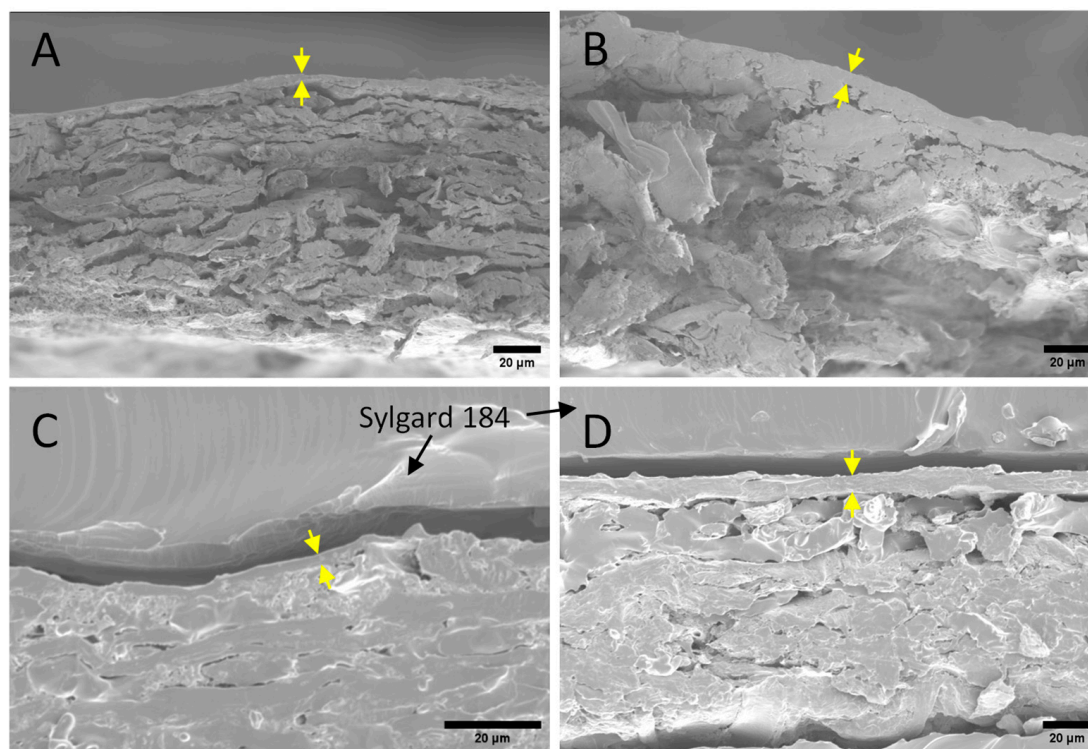
Figure 2. SEM micrographs of CNC- (**A**,**B**) and TOCN- (**C**,**D**) coated paper cross-sections: (**A**) doctor blade setting = 50 μm, dry coating thickness = 3.0 ± 0.4 μm, (**B**) doctor blade setting = 100 μm, dry thickness = 5.0 ± 0.4 μm, (**C**) doctor blade setting = 300 μm, dry thickness = 2.0 ± 0.2 μm, (**D**) doctor blade setting = 2000 μm, dry thickness = 8.2 ± 0.9 μm. Yellow arrows highlighting the coatings are included to guide the eye. Scale bars represent 20 μm.

3.1.2. Heptane Vapor Transmission of Neat Coatings

The differences in the barrier performance of cellulose nanomaterials directly coated on copy paper were evaluated, and TOCNs were found to generally have better barrier performance. For example, the heptane transmission was higher for the CNC-coated paper than the TOCN-coated paper at similar coating weights, especially between 2 and 8 g/m^2 coatings weights, as shown in Figure 3. At low coating weights, the variability in the HVTR was much higher than at higher coating weights, likely due to incomplete coating coverage. Koppolu et al. found significantly reduced heptane transmission rates of CNC-coated paperboard at lower coating weights than were observed here [20]. They found that the HVTR was reduced by an order of magnitude with a coating weight of 3.3 g/m^2 and by two orders of magnitude with a coating weight of 4.3 g/m^2. Here, we found an order of magnitude reduction with about 8–10 g/m^2 of CNCs. One reason for this difference may be that Koppolu et al. used base coatings on the paperboard. However, here, less than 2 g/m^2 of TOCNs was necessary to achieve an order of magnitude reduction in HVTRs. One primary difference between TOCNs and CNCs is their particle morphology. CNCs are discrete needle-shaped particles that are approximately 3–10 nanometers in diameter and about 100–300 nm in length [53,54]. TOCNs are continuous fibers with a similar diameter but can be up to several micrometers long [3,5,41,55]. The length and structure of the TOCNs allowed entangled networks of particles to form. This networked structure of TOCNs appears to have allowed the TOCNs to form a continuous film at lower coating weights than the CNCs. The discrete, short-length nature of the CNCs allowed them to sink into the porosity of the paper, making it harder for a continuous film to form. Adding plasticizers, polymers, or base layers may be able to improve the continuity of the film and thus the barrier performance of these coatings [20].
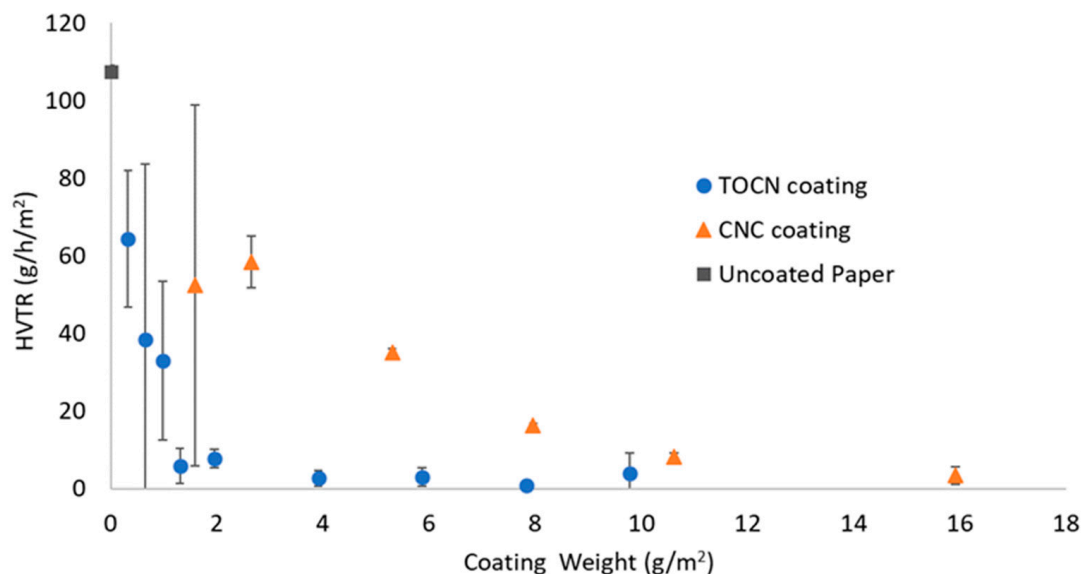
Figure 3. Heptane vapor transmission rates for copy paper coated with TOCNs or CNCs. Coating speed was 50 mm/s.

3.1.3. Grease Resistance of Neat Coatings

Grease resistance testing was performed for TOCN-, CNC-, and CMC-coated papers, and TOCNs were generally better barriers to canola oil than the CNCs or CMCs. Figure 4 shows that the amount of grease that penetrated coated copy paper was higher for the CNC and CMC coatings than the TOCN coatings. TOCN coatings of 2–3 g/m^2 were enough to essentially reduce the oil penetration of uncreased papers to zero. The grease penetration was still more than zero for the CNC-coated papers even above 10 g/m^2. As stated before, TOCNs appear to have better film-forming properties on porous paper substrates than CNCs due to the networked structures that form in TOCNs during drying. It also appears that the networked nature of TOCNs was better at forming continuous films than the polymer CMC, which is interesting because CMC is known for its high viscosity and film-forming properties. However, some penetration of CMC into the papers was observed, which makes it difficult for a continuous film to form and create a barrier to grease penetration. As seen in Figure 5A–C, at low coating weights of CMC, significant defects were observed. The CMC coatings with 50 μm and 100 μm doctor blade gaps had coating weights of approximately 6 g/m^2 and 11 g/m^2, respectively, but still appeared to have incomplete coverage; however, the coating done with a 300 μm doctor blade gap was a continuous and defect-free film with a weight of approximately 26 g/m^2. Therefore, high coating weights (somewhere above 11 g/m^2) of CMC may be required for continuous, defect-free films.

The grease penetration was significantly increased for the coated papers after the samples were creased with a double fold (Figure 6). In all cases, the dyed oil stained more than 20% of the receiving blotter paper after penetrating CNC-coated papers, even with over 12 g/m^2 of coating applied. The grease penetration of the creased TOCN-coated papers was more than zero even for the high coating weights, but the dyed area of the blotter paper was less than 5% for the high coating weights. The creased CMC-coated papers had similar grease penetration values as the TOCN- and CNC-coated papers. It appears that the brittle nature of all three coating materials results in films that cannot survive the TAPPI T512 creasing method. The only coatings that show some resistance to ceasing are the CMC coatings at relatively high coating weights of around 20 g/m^2. Cellulose nanomaterial films are known for their lack of ductility due to the high stiffness of their particles and strong molecular interactions between their particles. Larger dyed areas after creasing are indicative of cracking in the films during creasing that allowed grease through. If these materials are to be used in paper coating applications where creasing operations are required, then the durability of the created films must be enhanced. Possible enhancements in durability can be

achieved via the addition of plasticizers, more ductile water-soluble polymers, or a reduction in the residual stress that forms within the film during drying [56].
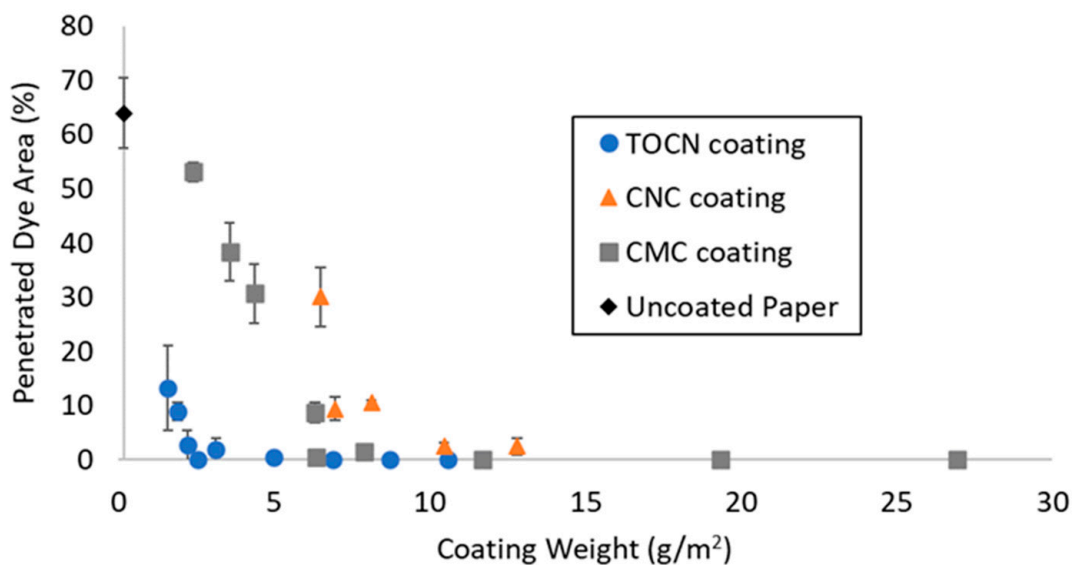

Figure 4. Grease penetration for uncreased paper samples. Coating speed was approximately 11 mm/s.
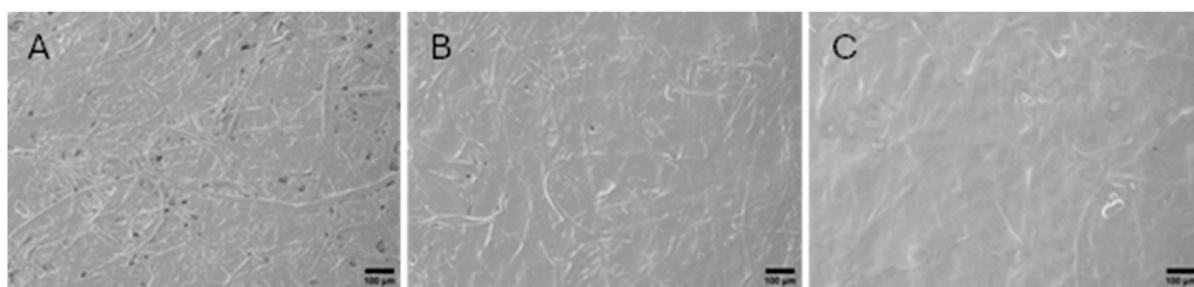

Figure 5. Electron micrographs of CMC coatings depicting the transition to full film formation as coating thickness increases. Approximate doctor blade settings: (**A**) 30 μm; (**B**) 100 μm; (**C**) 300 μm. Scale bars represent 100 μm.
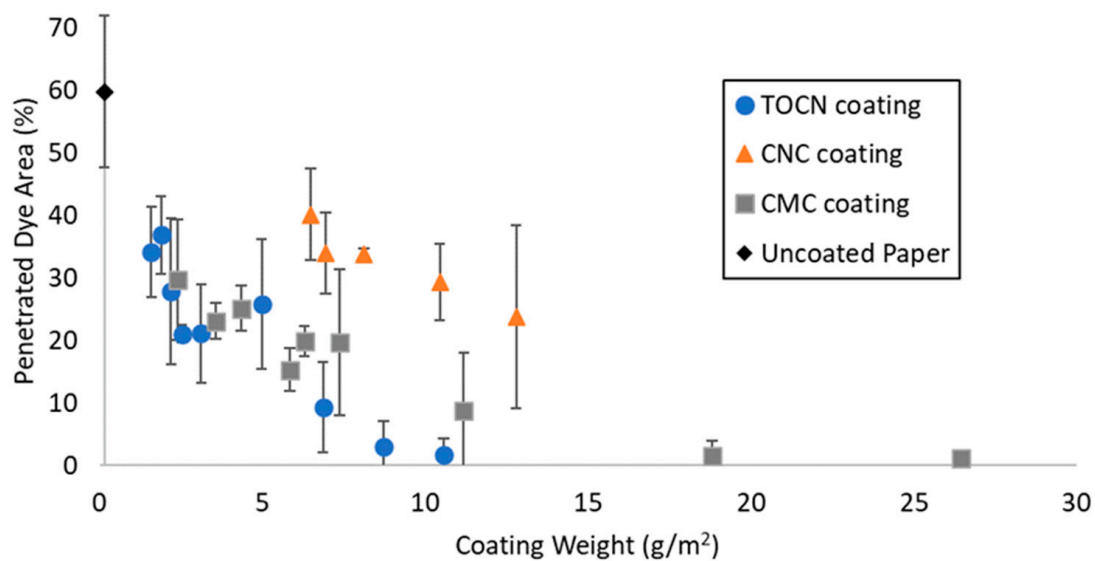

Figure 6. Grease penetration for creased paper samples. Coating speed was approximately 11 mm/s.

The grease-resistance testing of CNM-coated papers is typically performed using the TAPPI T559 testing kit [43], so the CNC and TOCN coatings were also evaluated for their kit rating. For the TOCN-coated papers, an average kit rating of 11.7 (out of 12) was found for heavy coatings of about 10 g/m^2, but the values were considerably lower for the moderate coatings. For the CNC-coated papers, the kit ratings were found to be much lower. For the papers coated with as-received CNCs, the highest average kit rating was about 1. The failures were typically seen as either pinholes or cracks. The paper was rarely stained by the entire drop of oil/solvent mixtures, as was the case when evaluating the uncoated papers. Therefore, the low kit ratings for the CNCs are likely due to defects, cracks, and non-uniform coverage. Tyagi et al. also found low kit ratings for cellulose nanomaterials coated directly onto bleached Kraft paper, with a kit rating of approximately 3 for CNCs and approximately 7 for CNFs [29]. They were able to improve the kit rating of coated papers by incorporating clay and protein into the nanocellulose, and they achieved the highest kit rating of 12 when applying a layer of CNF followed by a layer of a clay–protein–CNC mixture. In another example, Lavoine et al. found a maximum kit rating of 5 for fibrillated cellulose-coated papers [23]. Mazega found a kit rating of 8–9 for about 5 g/m^2 of TOCNs coated onto bleached calendered paper [57].

3.2. Effects of Processing Conditions

The effect of processing conditions such as the coating speed or dispersion methods on the coating performance has not been well studied. Cellulose nanomaterials are commonly sonicated to improve their dispersion [12,58–60], so the effect of sonication on their barrier properties was also evaluated. As shown in Figure 7, sonication of the CNC suspensions with about 1 kJ/g of energy resulted in some improvement in grease resistance, but even at coating weights above 12 g/m^2, the kit rating was only about 6. Beck et al. found that the sonication of CNCs led to increases in the resulting suspension chiral nematic pitch from about 3.4 μm without sonication to 15.7 μm with 1.3 kJ/g of sonication energy, which was similar to the 1 kJ/g used here [61]. Sonication hinders anisotropic phase formation and decreases the volume fraction of the chiral nematic phase [61]. Gicquel et al. note that the critical concentration at which phase separation occurs was increased with sonication [59]. The conductivity of suspensions was also increased, potentially screening or weakening chiral interactions [61]. These changes to the suspension affect the self-assembly of the CNCs in both suspensions and films and are hypothesized to result in larger domains with less residual stress and fewer defects. Further evaluations of this behavior are warranted.
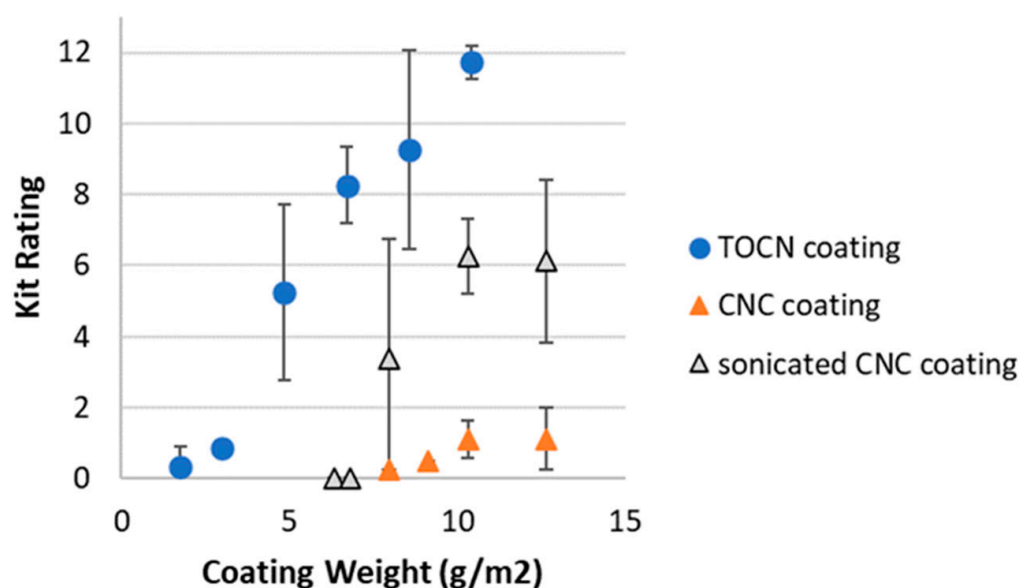

Figure 7. TAPPI kit rating for coated copy papers.

The air permeability of the tested copy papers with TOCNs with and without son-ication for two different wet blade thicknesses is shown in Figure 8. The sonication of TOCNs (at 10 kJ/g) resulted in significantly more permeable coatings than those of the non-sonicated samples. The main noticeable difference in the TOCN suspension after sonication was that the viscosity was dramatically reduced. Consequently, rheological measurements were used to evaluate the effect of sonication on the gel structure and flow.
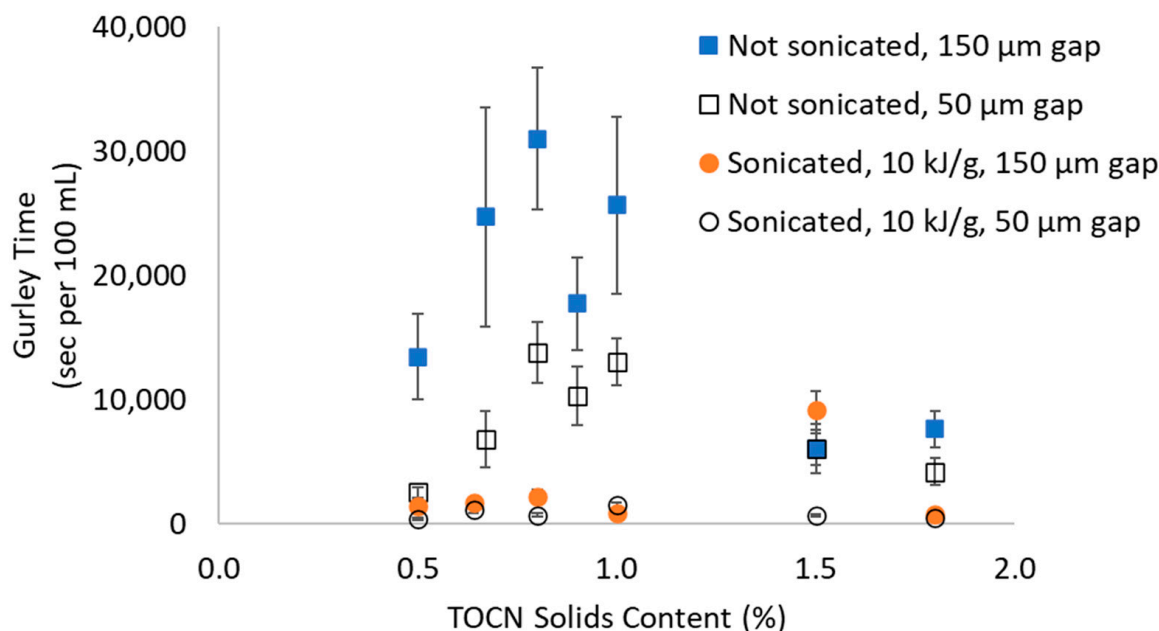

Figure 8. Effect of concentration and sonication on air permeability (coated side up) of TOCNs coated on copy paper (Copy1) at two different coating thicknesses. Coating speed was approximately 10 mm/s, and drying setpoint was 35 °C. Error bars represent standard error of the mean.

Amplitude sweeps were performed during the small-amplitude oscillatory shear (SAOS) testing of 1% TOCN suspensions with (10 kJ/g) and without sonication (Figure 9). The curves show features typical of gels such as the much higher storage versus loss moduli in the linear viscoelastic (LVE) region, and the peak in the loss moduli after the onset of yielding. At low amplitudes, the curves for different gap sizes for the sonicated suspensions overlap, but those for the non-sonicated suspensions trend downward as the gap thickness is reduced, which is evidence of wall slip or shear banding. These are common problems in the rheological testing of nanocellulose [62], which apparently were not entirely eliminated by the roughened contact surfaces when testing the non-sonicated suspension. Nevertheless, all storage moduli for the non-sonicated suspension were higher than those of the sonicated suspensions (Table 1). Also, greater shear stresses were found at the yield and flow points. These results suggest that the intense sonication permanently disrupted the gel structure.
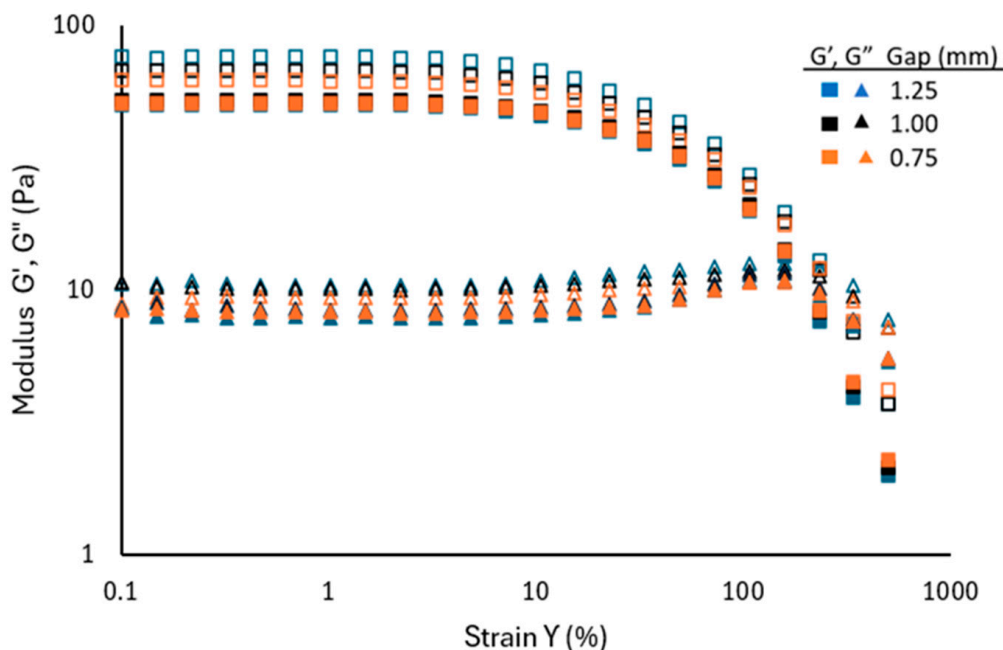
Figure 9. Amplitude sweeps from SAOS testing of 1% TOCN suspensions with (solid) and without (open) sonication.

Table 1. Specific values from amplitude sweeps during SAOS testing of sonicated and non-sonicated 1% TOCN suspensions.

Sonic. Level (kJ/g)	Gap Thickness (mm)	LVE Region [1]	Yield Point [2]		Flow Point	
		Storage Modulus (Pa)	Shear Strain (%)	Shear Stress (Pa)	Shear Strain (%)	Shear Stress (Pa)
0	1.25	76.3	6.4	3.7	247	42.6
0	1.00	67.9	6.3	3.3	245	38.5
0	0.75	62.4	6.4	3.0	283	38.7
10	1.25	50.5	7.0	2.5	191	27.7
10	1.00	52.4	7.1	2.6	191	29.6
10	0.75	51.1	7.1	2.5	202	29.3

[1] Tables may have a footer. [2] Yield point determined as the point at which there is a 5% reduction in storage modulus.

Three interval thixotropy tests (3ITT) were also performed on the suspensions (Figure 10). After initial characterization of the gel (first interval), the gels were sheared at 67, 200, or 500 s^{-1} for 5 min (second interval). The first two shear rates correspond to those used in coating the paper for the Gurley tests in Figure 3, albeit at a much larger gap size and for a much longer time than the material would experience during blade coating. The recovery of the gel was then evaluated by SAOS testing during the third interval. The viscosities of the sonicated suspensions were found to be lower at all stages of the test compared to the non-sonicated suspensions. Neither of the TOCN suspensions fully recovered their loss modulus, even 30 min after shearing. Also, the sonicated samples were more sensitive to shear rates than the non-sonicated samples, probably because of their weaker gel structure. Similar trends were found for the storage and loss moduli. Additionally, the storage moduli were higher than the loss moduli at all stages of testing, albeit less so immediately after shearing. Overall, the 3ITT results indicate that: (1) even low shear rates affect the network structures of both suspensions, (2) the recovery of the structure was limited in the short term, and (3) the weaker, sonicated gel was more sensitive to the shear rate.
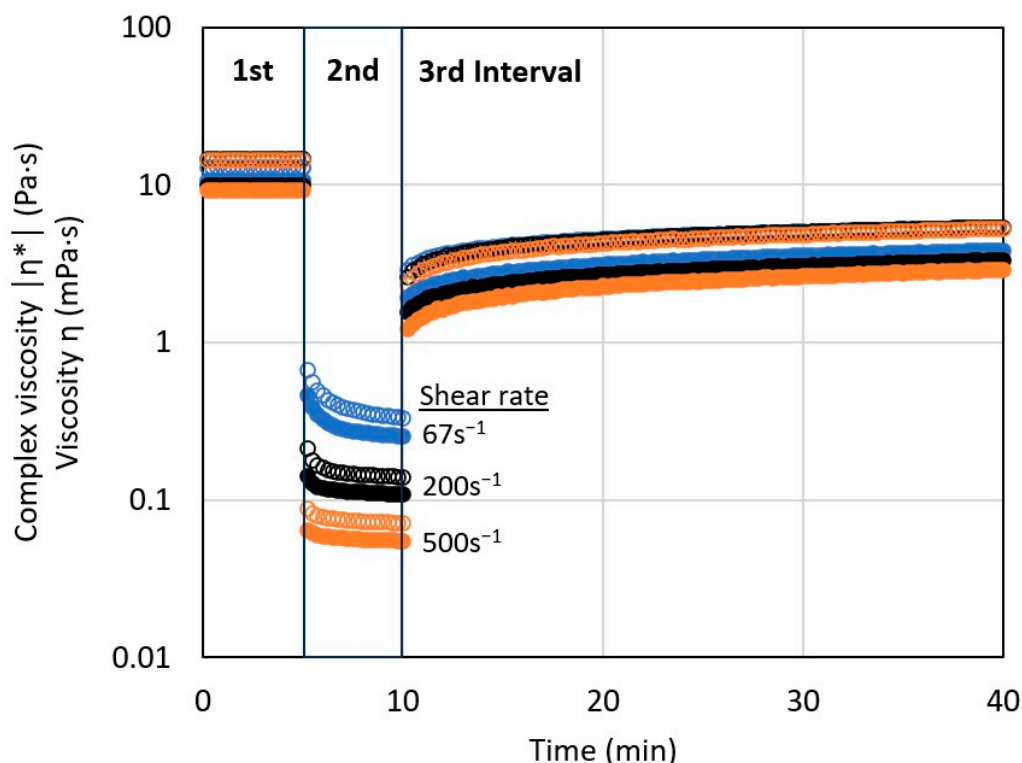
Figure 10. 3ITT of 1% TOCN suspensions with (solid) and without (open) sonication. Plate gap size was 1 mm. Interval 1 and 3: SAOS; interval 2: rotational.

Sonication was hypothesized to alter the morphology of TOCNs, so the apparent particle size and degree of polymerization were measured. Dynamic light scattering was used to evaluate the apparent particle size of TOCNs sonicated at various energy levels, as shown in Figure 11. Higher levels of sonication generally resulted in a decreased apparent size. The fiber lengths are expected to be shorter for sonicated samples, so smaller hydrodynamic diameters of TOCN fibers were expected. The samples sonicated at 10 kJ/g had an apparent particle size that was about 20% smaller than that of the non-sonicated samples. The degree of polymerization of the TOCNs was not as noticeably different, with a DP of 182 $\pm$ 4 for the non-sonicated TOCNs and 177 $\pm$ 5 for the TOCNs sonicated at 10 kJ/g. Changes in the fiber morphology alone do not seem to explain the dramatically different air permeability values observed for the sonicated and non-sonicated samples. Electron micrographs of the coated paper samples indicated that the sonicated samples exhibited cracking more commonly than the non-sonicated samples (Figure 12). These cracks may be a result of a decreased fiber morphology and/or the disruption of longer-range network structures. Additional work is needed to better understand the effects of fiber and suspension conditions on film formation.

Figure 8 also shows the effect of the solids concentration in the TOCN suspension on the air permeability. Not surprisingly, the samples with low and high concentrations generally did not perform as well as the samples with concentrations near 1%. The samples with concentrations above 1% generally did not flow well, so non-uniform coverage was observed. At low concentrations (e.g., 0.5%), less cellulose was available for coverage, so those samples generally had lower Gurley values. The coating weight was not measured for all samples, but typical coating weights for similar coating conditions were found to be about 1.4 and 2.1 g/m^2 for doctor blade gaps of approximately 50 and 150 μm. The Gurley time for the uncoated copy paper was only about 11 s, while it was up to 30,000 s for the coated copy paper. Depending on the substrate used, Aulin et al. measured from about four to five order of magnitude changes in porosity of samples coated with 1–2 g/m^2 of CNFs, which they referred to as MFC [9].
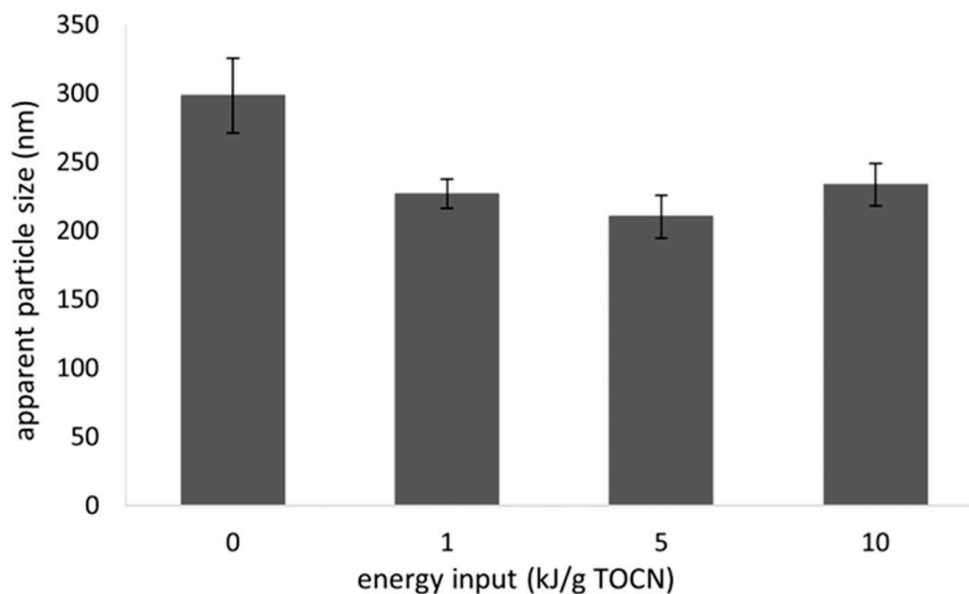
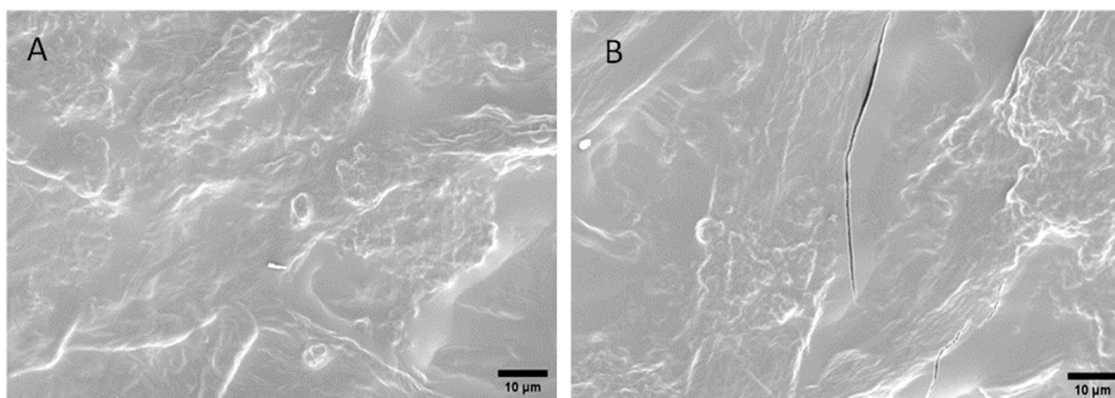**Figure 11.** Effective diameter for TOCNs at different sonication levels by DLS.

Figure 12. Electron micrograph of TOCN-coated paper surface without sonication (**A**) and with 10 kJ/g of sonication (**B**). Scale bars represent 10 μm.

The coating speed had a significant effect on the air permeability of the TOCN-coated papers, as shown in Figure 13. Extremely slow coating speeds (approximately 0.9 mm/s) were found to result in higher permeability, corresponding to much lower Gurley air resistance values (231 ± 34 s/100 mL for a doctor blade gap of about 50 μm) than all other speed conditions. The least permeable samples with the maximum Gurley values (12,900 ± 2900 s/100 mL for a doctor blade gap of about 50 μm) were found to be the samples coated at 10 mm/s. Higher coating speeds (e.g., 96 mm/s) resulted in values of 1360 ± 250 s/100 mL for a doctor blade gap of about 50 μm. Note that uncoated copy paper has Gurley values in the order of about 10 s, so the value of the coated papers was improved up to about 1000 times when coated with 1% TOCN suspensions with wet blade thicknesses of 50 to 150 μm, resulting in coating weights of approximately 1–3 g/m². The performance differences for the different operating conditions may likely be related to substrate distortions. As shown in Figure 14, the surfaces of the papers coated at slow speeds consistently had more wrinkles than the samples coated at faster speeds, which may be due to a longer residence time leading to more water soaking into the paper. Figure 14B,F depict SEM micrographs taken across the wrinkles of papers coated with two different doctor blade thicknesses at the low-speed setting. The surfaces of the wrinkles showed significant cracking in the coating, which was not observed in papers coated at higher speeds. These defects likely lead to the observed increase in air permeability of the papers

coated at slower speeds. The drying air temperature did not have significant impacts on the air resistance, as shown in Figure 15. Air permeability results are challenging to compare across the literature because air permeability test methods take a variety of forms and are often reported in drastically different manners. For example, Gicquel et al. [32] reported an "intrinsic permeability" in nm^2 using ISO standard 5636. In that work, they noted that cracks and defects affected barrier properties, especially for CNC coatings, and they found that multiple coatings led to better air barriers than single coatings [32]. The current results show that the coated papers had Gurley values 1000 times higher than the uncoated papers, while many of the results in the literature demonstrate much smaller changes [23,24,32].
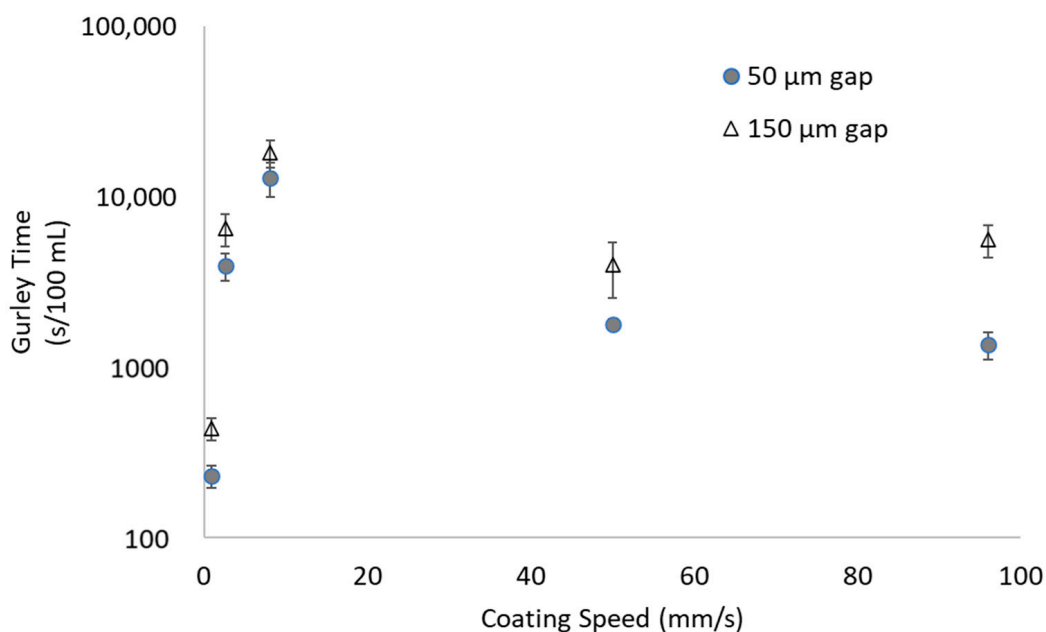

Figure 13. Effect of coating speed on air permeability of TOCN-coated copy paper. Drying setpoint was 35 °C. The value of uncoated papers was about 10 s. Error bars represent standard error of the mean.
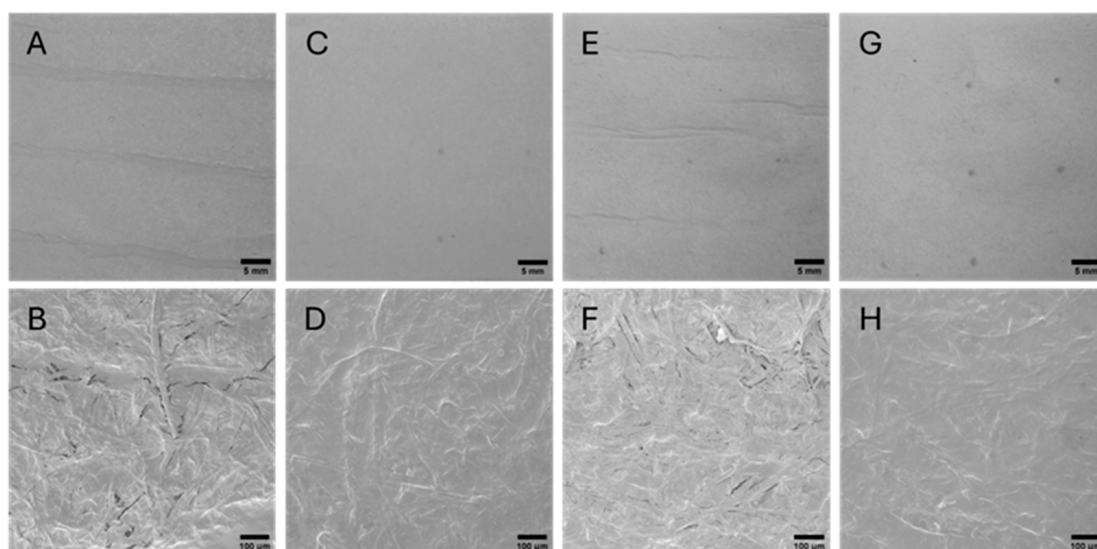

Figure 14. Optical (**top** row, scale bars represent 5 mm) and SEM micrographs (**bottom** row, scale bars represent 100 μm) of TOCN-coated papers demonstrating increased wrinkling and cracking in the coating at lower coating speeds for different doctor blade settings. (**A**,**B**) doctor blade = 50 μm, speed = 0.9 mm/s; (**C**,**D**) doctor blade = 50 μm, speed = 8 mm/s; (**E**,**F**) doctor blade = 150 μm, speed = 0.9 mm/s; (**G**,**H**) doctor blade = 150 μm, speed = 8 mm/s.
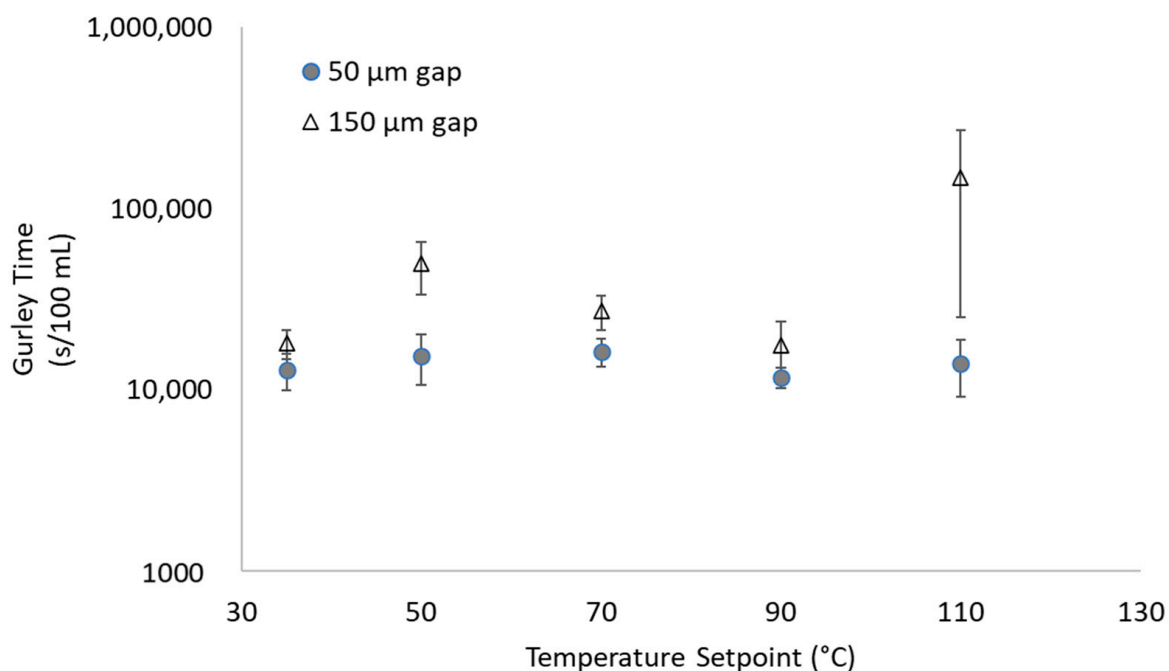
Figure 15. Effect of drying temperature setpoint on air permeability of TOCN-coated copy paper. Coating speed setpoint was 10 mm/s. Doctor blade gap was approximately 50 μm.

3.3. Coatings Containing Both Cellulose Nanomaterials and CMC

Carboxymethyl cellulose (CMC) has been used along with cellulose nanomaterials for paper coatings [20,24,35], but little information exists about the barrier properties of CMC itself. However, papers coated with CMC were shown to have low permeability [20,24]. He et al. also found good barrier properties for CMC–CNC-based coatings. Here, we have incorporated CMC into suspensions of CNCs or TOCNs to attempt to improve the barrier performance and durability of nanocellulose coatings and to minimize CNC penetration into the paper. When adding 250,000 MW of CMC to as-received CNC suspensions with about a 10.6% solids content, the viscosity was too high to readily mix them with impeller stirrers, so the mixture was diluted. The effect of the solids content on the Gurley times is shown in Figure 16. In general, higher solid contents led to better barriers. CNCs and TOCNs were also mixed with CMC at about 1% solid loadings, and papers were coated with the mixtures. The Gurley times of papers coated with the mixtures are shown in Figure 17. The values for commercial papers are also shown for comparison. Aside from the CNC–CMC coatings below 5 g/m^2, both the TOCN–CMC and CNC–CMC coatings had Gurley times in the same order of magnitude as the commercial papers, but the TOCN–CMC coatings generally had higher resistance to air than the CNC–CMC coatings. Note that the CNC coatings without CMC had significantly lower Gurley times, with a maximum average of less than 4000 s even for coatings of approximately 10 g/m^2. CMC appears to help prevent CNCs from penetrating into the paper and may fill in some voids, leading to improved air permeability. However, the addition of CMC did not appear to improve the grease resistance of CNCs or TOCNs, as grease penetration was still observed at similar coating levels with or without CMC.
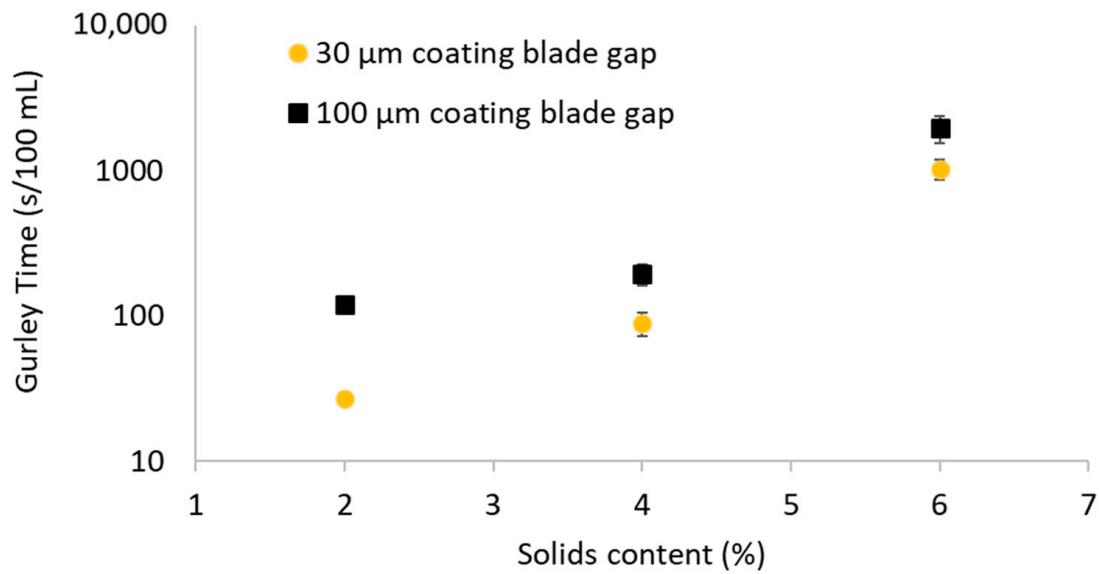
Figure 16. Air permeability of CNC–CMC-coated copy paper (Copy2) as a function of suspension solids content at two different coating thicknesses. Coating speed of 10 mm/s and drying setpoint of 35 C. Error bars represent standard error of the mean.
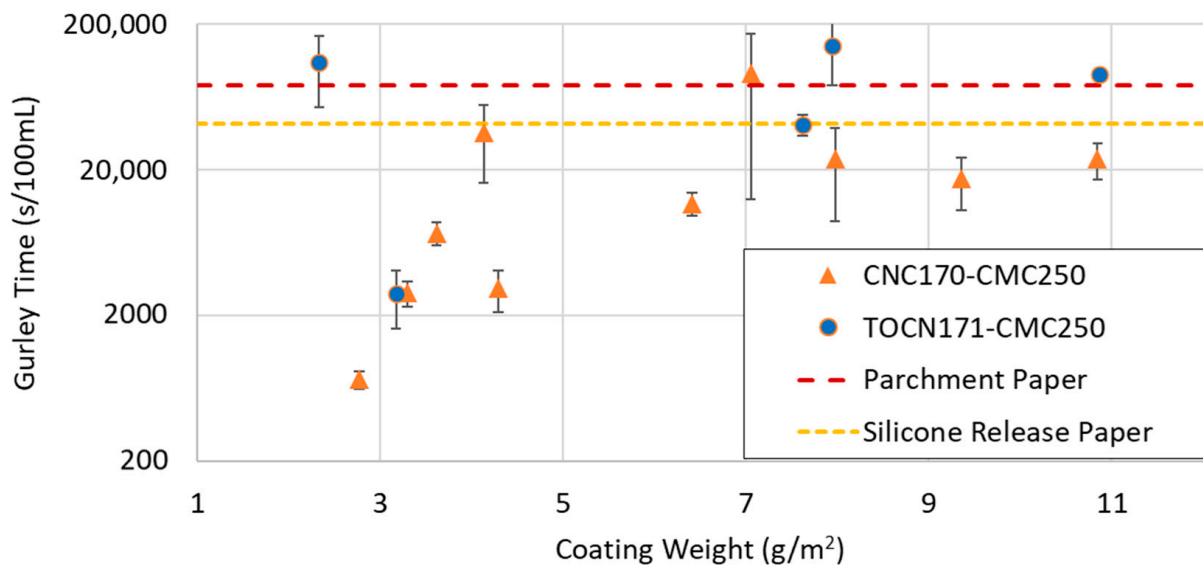

Figure 17. Air permeability of papers coated with mixtures of nanocellulose and CMC.

The oxygen permeability was also evaluated for papers coated with mixtures of nanocellulose and CMC. The papers coated with CNC–CMC mixtures were found to have oxygen transmission values above the detection limit of the instrument and were considered failures. This suggests that the contribution of the CMC was not substantial enough to provide the CNCs with the ability to form a continuous film on the surface of the paper. Cast films of CNCs provide good oxygen barrier properties; therefore, the process of coating the material on the paper lead to the defects that allowed oxygen to transmit through the paper. The papers coated with TOCN–CMC mixtures generally had good oxygen barrier properties, as displayed in Figure 18, which also shows the oxygen permeability of the cast films of TOCN–CMC. The samples were clearly moisture-sensitive, with values at 90% RH that were approximately three orders of magnitude higher than those at 10% RH, similar to the cast films of TOCN–CMC. The molecular weight of CMC did not appear to have a significant effect on the oxygen permeability, since coatings with 90,000 and 250,000 MW had similar

values across the range of humidities that was evaluated. Both the OTR and oxygen permeability were about an order of magnitude higher for the coated papers than for the cast films. However, note that the oxygen permeability values are normalized for the sample thickness, but how to determine the proper thickness to use for coated samples is not clear. In this case, the entire thickness of the paper (i.e., paper + coating) was used for the permeability calculations. The coatings, however, only constitute a small portion (approximately 10%) of the paper thickness. Therefore, the higher OTRs and oxygen permeability of the coated papers compared to the cast films is likely due to differences in the thicknesses of the barrier layers, not any defects or problems with the coating process.
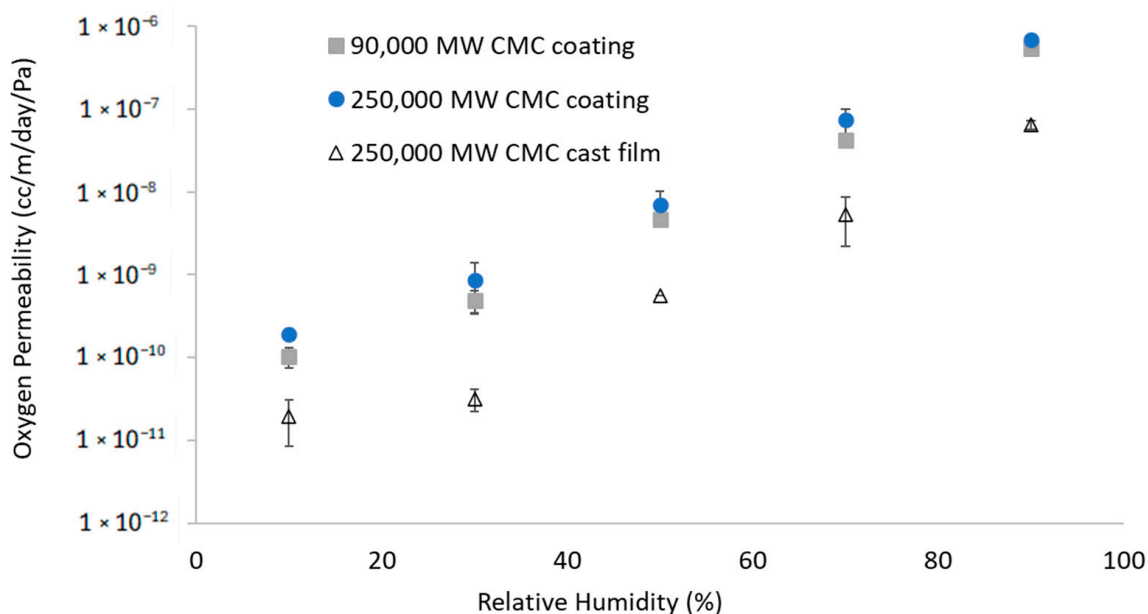

Figure 18. Oxygen permeability of TOCN–CMC-coated papers with either 90,000 or 250,000 CMC molecular weight and cast films. CMC:CNF ratio was 1:10. The papers were coated with a doctor blade gap of 1 mm.

3.4. Oxygen Transmission of Cast Films

Oxygen transmission measurements were also taken on copy paper coated with neat CNCs or TOCNs, but the OTR was beyond the range of the instrument, resulting in failed tests. With a 5 cm^2 mask, the maximum OTR of the instrument is about 2500 cm^3/m^2/day. The copy papers coated with unmodified cellulose nanomaterials were not found to be good oxygen barriers in this work, although, as shown in Figure 18, adding polymers can yield coated papers with good oxygen barriers. It is hypothesized that the continuity of the neat CNM films formed on top of porous copy paper is not sufficient enough to produce an effective barrier to oxygen. However, neat TOCN coated on other substrates was found to create good oxygen barriers. For example, the OTR of TOCN coated on silicone-coated release paper was 2.1 ± 1.1 cm^3/m^2/day at 50% RH and 3800 ± 200 cm^3/m^2/day at 90% RH. In other recent work, measurements of neat TOCN coated on calendered paper with a starch base layer had low oxygen transmission values of about 2–13 cm^3/m^2/day [56].

To evaluate the potential to create strong oxygen barriers without the influence of the substrate, films of neat CNCs or TOCNs were cast and evaluated for their oxygen permeability versus CMC films (Figure 19). The permeability of the cast TOCN films was generally lower than that of cast CNC films, especially below 90% RH. It is not clear why the CNC films had orders of magnitude higher oxygen transmission at low humidity levels than the CMC or TOCN films. Films of neat CNCs are typically brittle and readily damaged, so limited data are available in the literature on their oxygen permeability, especially over a range of humidity levels. A literature review by Ilyas et al. suggests that there may be a relationship between the oxygen permeability and stretchability of bio-composite films

reinforced with nanocellulose, so the use of added polymers or additional layers may also improve the oxygen permeability by improving the mechanical integrity of barrier coatings [63]. Martinez-Sanz reported that CNCs from bacterial cellulose had oxygen permeability coefficients that were four orders of magnitude higher at 80% RH than at 0% RH [64]. CNC films at low humidity are expected to be less swollen than those at high humidity, and these films at low humidity may contain defects or have structures that do not facilitate intimate bonding of the CNCs. The method of preparing the films is expected to impact the structure, so future examination of the oxygen permeability behavior of CNC films produced under different conditions is warranted.
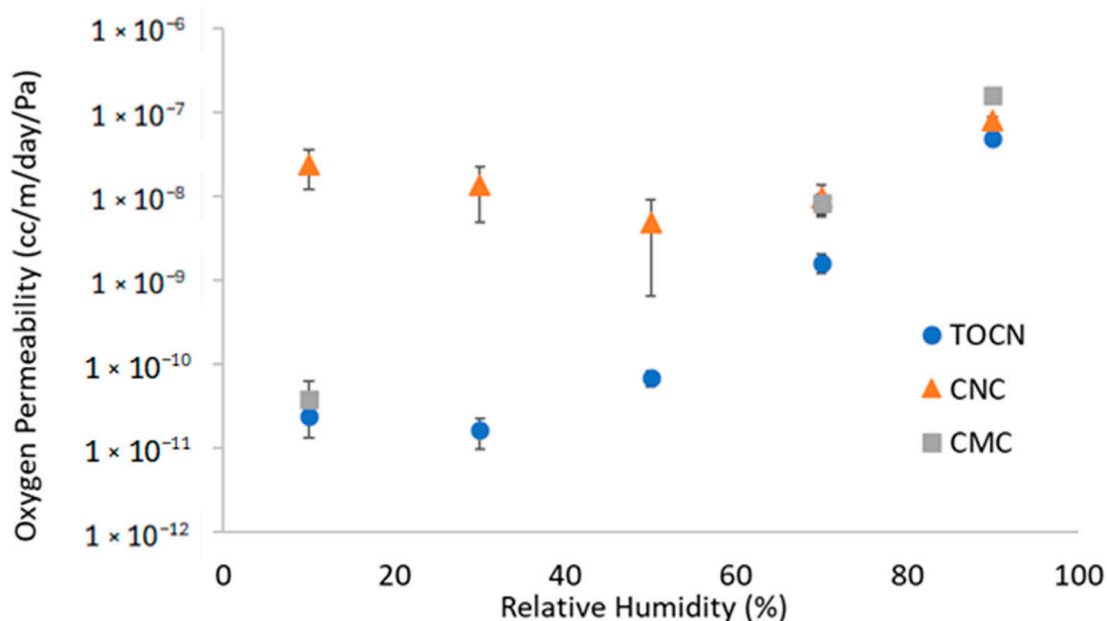

Figure 19. Oxygen permeability of cast films of TOCNs or CNCs. Error bars represent standard error of the mean.

3.5. Oxygen Transmission of Multilayer Films

The results of oxygen transmission testing suggest that it is difficult to achieve an oxygen barrier material by applying neat cellulose nanomaterials directly to paper substrates. Table 2 shows the oxygen transmission results for 10 g/m^2 coatings on copy paper. Neat cellulose nanocrystals appeared to sink into the paper upon application, resulting in pinholes in the film that oxygen could pass through easily (failed oxygen test). Even the addition of CMC did not appear to allow the CNCs to form a continuous film when coated onto porous paper. The morphology of the high aspect ratio and flexible fibers of TOCNs appear to help them form a long-range networked structure that results in a more continuous film upon drying. However, the TOCNs still result in a brittle film, and drying stresses may result in cracks that prevent them from forming an oxygen barrier on paper. The only material that resulted in a successful oxygen barrier when applied to porous copy paper was the combination of TOCNs mixed with CMC. It is hypothesized that the CMC provides enough durability to the TOCNs that a continuous film can form on the paper without cracking. The CMC could also aid in film formation through eliciting an increased viscosity of the suspension. The combination of TOCNs and CMC at 10 g/m^2 provides an oxygen barrier that is adequate for a wide range of food packaging applications at low humidities. As shown in the prior literature, at high humidity levels, cellulose nanomaterials are not sufficient for more stringent food applications, such as coffee or potato chip bags.

Table 2. Oxygen transmission rates in cm^3/m^2·day for 10 g/m^2 coatings of cellulose nanomaterials by themselves and with a secondary application of a commercial water vapor barrier material.

Sample Type	Relative Humidity	Without Water Barrier	With Water Barrier
TOCN	30%	Failed	1.7 ± 0.1
	70%	Failed	61.0 ± 5.4
CNC	30%	Failed	139 ± 71
	70%	Failed	212 ± 65
TOCN-CMC	30%	0.71 ± 0.67	1.5 ± 0.1
	70%	61.2 ± 36.5	50.2 ± 5.4
CNC-CMC	30%	Failed	4.2 ± 1.1
	70%	Failed	74.3 ± 7.6

The highly hydrophilic nature of cellulose nanomaterials suggests that, when used in a food packaging application, an additional water vapor barrier or water contact layer may be needed in addition to the cellulose oxygen barrier layer. In this work, the oxygen transmission of the nanocellulose coatings on paper was examined after the addition of a secondary proprietary commercial water vapor barrier (Melodea VBCoat®, Shfella Area, Israel) material. Interestingly, when adding the secondary layer, the cellulose coatings (that failed oxygen transmission testing when used alone) became useful oxygen barriers. Both the neat TOCNs and CNCs with CMC provided oxygen barriers that were suitable for most food packaging applications once the secondary water vapor barrier was added. The water vapor barrier material is not known to be a good oxygen barrier, as the oxygen transmission of papers coated only with the water barrier was beyond the test limit of the instrument and, therefore, it does not add to the oxygen resistance directly. The water barrier coating likely contains surfactants and polymers that may interact with the cellulose, rearranging the particles or creating more flexible and durable coating layers. This likely resulted in cracks or pinholes that formed in the initial nanocellulose layer being filled, thus cutting off the easy transmission path for oxygen molecules. The synergy of these layers resulting in good barrier performance is of strong practical significance, and further investigation into the mechanisms of how double-layer coatings work is warranted. Note that applying a second layer of nanocellulose did not result in improved oxygen barriers of the coated copy papers. The double-layer samples were also creased, but their oxygen transmission levels were above the instrument's maximum detection limit. Therefore, more work is needed to produce coatings with enhanced durability.

4. Conclusions

The barrier performance of copy papers coated with cellulose nanocrystals, cellulose nanofibrils, and carboxymethyl cellulose was examined. The CNCs did not perform well by themselves as they tended to soak into the paper, preventing them from forming a film. Their discrete particle morphology makes it difficult for continuous networks and thus films to form. The morphology of the TOCN particles allowed networked structures to form, which helped the material remain on the surface of the paper and form more coherent films. The film formation and barrier properties were enhanced on nanocellulose-coated papers when CMC was added. Additionally, a base layer may also assist in continuous film formation by preventing the nanomaterials from soaking into the paper. The processing conditions were also found to have a significant impact on barrier properties, although these effects are not yet well understood. In some cases, such as at a low coating speed, the resulting poor performance appeared to be related to distortion of the substrate, and, in others, cracking and defects were observed. The sonication of TOCNs resulted in reduced barrier performance, likely due to a decreased fiber size and the disruption of long-range network structures. The sonication of CNCs modestly improved their performance as barrier coatings, but they still did not perform as well as TOCNs. Adding water barrier coatings to

nanocellulose-coated papers was found to further improve their barrier properties, even though the water barrier coating itself was not a good barrier to oxygen. The synergy of these multi-layer constructs deserves further investigation to produce films with good water, oxygen, air, and grease barriers.

Author Contributions: Conceptualization, R.S.; methodology, R.S., C.S., C.C., D.F., N.R.G., M.L., K.H. and P.K.; writing—original draft preparation, R.S., C.S., C.C. and D.F.; writing—review and editing, R.S., C.S., C.C., D.F. and N.R.G.; project administration, R.S.; funding acquisition, R.S. All authors have read and agreed to the published version of the manuscript.

Institutional Review Board Statement: Not applicable.

Data Availability Statement: Data from this research is available from the USDA Forest Service, Forest Products Laboratory and is administered by Ronald Sabo.

Conflicts of Interest: The authors declare no conflicts of interest.

References

1. Williams, A.T.; Rangel-Buitrago, N. The past, present, and future of plastic pollution. *Mar. Pollut. Bull.* **2022**, *176*, 113429. [CrossRef] [PubMed]
2. Ahankari, S.S.; Subhedar, A.R.; Bhadauria, S.S.; Dufresne, A. Nanocellulose in food packaging: A review. *Carbohydr. Polym.* **2021**, *255*, 117479. [CrossRef] [PubMed]
3. Wang, J.; Gardner, D.J.; Stark, N.M.; Bousfield, D.W.; Tajvidi, M.; Cai, Z. Moisture and oxygen barrier properties of cellulose nanomaterial-based films. *ACS Sustain. Chem. Eng.* **2018**, *6*, 49–70. [CrossRef]
4. Nair, S.S.; Zhu, J.Y.; Deng, Y.; Ragauskas, A.J. High performance green barriers based on nanocellulose. *Sustain. Chem. Process.* **2014**, *2*, 23. [CrossRef]
5. Hubbe, M.A.; Ferrer, A.; Tyagi, P.; Yin, Y.; Salas, C.; Pal, L.; Rojas, O.J. Nanocellulose in thin films, coatings, and plies for packaging applications: A review. *BioResources* **2017**, *12*, 2143–2233. [CrossRef]
6. Lavoine, N.; Desloges, I.; Dufresne, A.; Bras, J. Microfibrillated cellulose—Its barrier properties and applications in cellulosic materials: A review. *Carbohydr. Polym.* **2012**, *90*, 735–764. [CrossRef]
7. Chi, K.; Catchmark, J.M. Improved eco-friendly barrier materials based on crystalline nanocellulose/chitosan/carboxymethyl cellulose polyelectrolyte complexes. *Food Hydrocoll.* **2018**, *80*, 195–205. [CrossRef]
8. Qing, Y.; Sabo, R.; Wu, Y.; Cai, Z. Resin Impregnation of Cellulose Nanofibril Films Facilitated by Water Swelling. *Cellulose* **2013**, *20*, 303–313. [CrossRef]
9. Aulin, C.; Gällstedt, M.; Lindström, T. Oxygen and oil barrier properties of microfibrillated cellulose films and coatings. *Cellulose* **2010**, *17*, 559–574. [CrossRef]
10. Belbekhouche, S.; Bras, J.; Siqueira, G.; Chappey, C.; Lebrun, L.; Khelifi, B.; Marais, S.; Dufresne, A. Water sorption behavior and gas barrier properties of cellulose whiskers and microfibrils films. *Carbohydr. Polym.* **2011**, *83*, 1740–1748. [CrossRef]
11. Hasan, I.; Wang, J.; Tajvidi, M. Tuning physical, mechanical and barrier properties of cellulose nanofibril films through film drying techniques coupled with thermal compression. *Cellulose* **2021**, *28*, 11345–11366. [CrossRef]
12. Fotie, G.; Gazzotti, S.; Ortenzi, M.A.; Piergiovanni, L. Implementation of high gas barrier laminated films based on cellulose nanocrystals for food flexible packaging. *Appl. Sci.* **2020**, *10*, 3201. [CrossRef]
13. Rampazzo, R.; Alkan, D.; Gazzotti, S.; Ortenzi, M.A.; Piva, G.; Piergiovanni, L. Cellulose nanocrystals from lignocellulosic raw materials, for oxygen barrier coatings on food packaging films. *Packag. Technol. Sci.* **2017**, *30*, 645–661. [CrossRef]
14. Chowdhury, R.A.; Nuruddin, M.; Clarkson, C.; Montes, F.; Howarter, J.; Youngblood, J.P. Cellulose nanocrystal (CNC) coatings with controlled anisotropy as high-performance gas barrier films. *ACS Appl. Mater. Interfaces* **2019**, *11*, 1376–1383. [CrossRef]
15. Mascheroni, E.; Rampazzo, R.; Ortenzi, M.A.; Piva, G.; Bonetti, S.; Piergiovanni, L. Comparison of cellulose nanocrystals obtained by sulfuric acid hydrolysis and ammonium persulfate, to be used as coating on flexible food-packaging materials. *Cellulose* **2016**, *23*, 779–793. [CrossRef]
16. Cozzolino, C.A.; Campanella, G.; Türe, H.; Olsson, R.T.; Farris, S. Microfibrillated cellulose and borax as mechanical, O_2-barrier, and surface-modulating agents of pullulan biocomposite coatings on BOPP. *Carbohydr. Polym.* **2016**, *143*, 179–187. [CrossRef]
17. Wang, L.; Chen, C.; Wang, J.; Gardner, D.J.; Tajvidi, M. Cellulose nanofibrils versus cellulose nanocrystals: Comparison of performance in flexible multilayer films for packaging applications. *Food Packag. Shelf Life* **2020**, *23*, 100464. [CrossRef]

18. Vähä-Nissi, M.; Koivula, H.M.; Räisänen, H.M.; Vartiainen, J.; Ragni, P.; Kenttä, E.; Kaljunen, T.; Malm, T.; Minkkinen, H.; Harlin, A. Cellulose nanofibrils in biobased multilayer films for food packaging. *J. Appl. Polym. Sci.* **2017**, *134*, 44830. [CrossRef]
19. Vartiainen, J.; Shen, Y.; Kaljunen, T.; Malm, T.; Vähä-Nissi, M.; Putkonen, M.; Harlin, A. Bio-based multilayer barrier films by extrusion, dispersion coating and atomic layer deposition. *J. Appl. Polym. Sci.* **2016**, *133*, 42260. [CrossRef]
20. Koppolu, R.; Abitbol, T.; Kumar, V.; Jaiswal, A.K.; Swerin, A.; Toivakka, M. Continuous roll-to-roll coating of cellulose nanocrystals onto paperboard. *Cellulose* **2018**, *25*, 6055–6069. [CrossRef]
21. Koppolu, R.; Lahti, J.; Abitbol, T.; Swerin, A.; Kuusipalo, J.; Toivakka, M. Continuous processing of nanocellulose and polylactic acid into multilayer barrier coatings. *ACS Appl. Mater. Interfaces* **2019**, *11*, 11920–11927. [CrossRef] [PubMed]
22. Du, P.; Ding, Q.; Zhao, C.; Jiang, Y.; Han, W.; Li, X. The fluorine-free coating has excellent hydrophobic and oleophobic properties for porous cellulose-based materials. *Cellulose* **2021**, *28*, 6133–6146. [CrossRef]
23. Lavoine, N.; Desloges, I.; Khelifi, B.; Bras, J. Impact of different coating processes of microfibrillated cellulose on the mechanical and barrier properties of paper. *J. Mater. Sci.* **2014**, *49*, 2879–2893. [CrossRef]
24. He, Y.; Li, H.; Fei, X.; Peng, L. Carboxymethyl cellulose/cellulose nanocrystals immobilized silver nanoparticles as an effective coating to improve barrier and antibacterial properties of paper for food packaging applications. *Carbohydr. Polym.* **2021**, *252*, 117156. [CrossRef] [PubMed]
25. Fukuzumi, H.; Saito, T.; Iwata, T.; Kumamoto, Y.; Isogai, A. Transparent and High Gas Barrier Films of Cellulose Nanofibers Prepared by TEMPO-Mediated Oxidation. *Biomacromolecules* **2009**, *10*, 162–165. [CrossRef]
26. Fukuzumi, H.; Saito, T.; Isogai, A. Influence of TEMPO-oxidized cellulose nanofibril length on film properties. *Carbohydr. Polym.* **2013**, *93*, 172–177. [CrossRef]
27. Hossain, R.; Tajvidi, M.; Bousfield, D.; Gardner, D.J. Multi-layer oil-resistant food serving containers made using cellulose nanofiber coated wood flour composites. *Carbohydr. Polym.* **2021**, *267*, 118221. [CrossRef]
28. Tyagi, P.; Hubbe, M.A.; Lucia, L.; Pal, L. High performance nanocellulose-based composite coatings for oil and grease resistance. *Cellulose* **2018**, *25*, 3377–3391. [CrossRef]
29. Tyagi, P.; Lucia, L.A.; Hubbe, M.A.; Pal, L. Nanocellulose-based multilayer barrier coatings for gas, oil, and grease resistance. *Carbohydr. Polym.* **2019**, *206*, 281–288. [CrossRef]
30. Tayeb, A.H.; Tajvidi, M.; Bousfield, D. Paper-based oil barrier packaging using lignin-containing cellulose nanofibrils. *Molecules* **2020**, *25*, 1344. [CrossRef]
31. Ruberto, Y.; Vivod, V.; Grkman, J.J.; Lavrič, G.; Graiff, C.; Kokol, V. Slot-die coating of cellulose nanocrystals and chitosan for improved barrier properties of paper. *Cellulose* **2024**, *31*, 3589–3606. [CrossRef]
32. Gicquel, E.; Martin, C.; Garrido Yanez, J.; Bras, J. Cellulose nanocrystals as new bio-based coating layer for improving fiber-based mechanical and barrier properties. *J. Mater. Sci.* **2017**, *52*, 3048–3061. [CrossRef]
33. Herrera, M.A.; Mathew, A.P.; Oksman, K. Barrier and mechanical properties of plasticized and cross-linked nanocellulose coatings for paper packaging applications. *Cellulose* **2017**, *24*, 3969–3980. [CrossRef]
34. Rahman, M.S.; Hasan, M.S.; Nitai, A.S.; Nam, S.; Karmakar, A.K.; Ahsan, M.S.; Shiddiky, M.J.A.; Ahmed, M.B. Recent developments of carboxymethyl cellulose. *Polymers* **2021**, *13*, 1345. [CrossRef]
35. Basta, A.H.; Khwaldia, K.; Aloui, H.; El-Saied, H. Enhancing the performance of carboxymethyl cellulose by chitosan in producing barrier coated paper sheets. *Nord. Pulp Pap. Res. J.* **2015**, *30*, 617–625. [CrossRef]
36. Li, F.; Biagioni, P.; Bollani, M.; Maccagnan, A.; Piergiovanni, L. Multi-functional coating of cellulose nanocrystals for flexible packaging applications. *Cellulose* **2013**, *20*, 2491–2504. [CrossRef]
37. Tayeb, A.H.; Tajvidi, M. Sustainable barrier system via self-assembly of colloidal montmorillonite and cross-linking resins on nanocellulose interfaces. *ACS Appl. Mater. Interfaces* **2019**, *11*, 1604–1615. [CrossRef]
38. Chen, C.; Sun, W.; Wang, L.; Tajvidi, M.; Wang, J.; Gardner, D.J. Transparent multifunctional cellulose nanocrystal films prepared using trivalent metal ion exchange for food packaging. *ACS Sustain. Chem. Eng.* **2022**, *10*, 9419–9430. [CrossRef]
39. Reiner, R.S.; Rudie, A.W. Process Scale-Up of Cellulose Nanocrystal Production to 25 kg per Batch at the Forest Products Laboratory. In *Production and Application of Cellulose Nanomaterials*; Postek, M.T., Moon, R.J., Rudie, A.W., Bilodeau, M.A., Eds.; Tappi Press: Atlanta, GA, USA, 2013; pp. 21–24.
40. Reiner, R.S.; Rudie, A.W. Experiences with scaling-up production of TEMPO-grade cellulose nanofibrils. In *Nanocelluloses: Their Preparation, Properties, and Applications*; ACS Publications: Washington, DC, USA, 2017; pp. 227–245.
41. Saito, T.; Kimura, S.; Nishiyama, Y.; Isogai, A. Cellulose Nanofibers Prepared by TEMPO-Mediated Oxidation of Native Cellulose. *Biomacromolecules* **2007**, *8*, 2485–2491. [CrossRef]
42. TAPPI. *T 507 cm-22 Grease Resistance of Flexible Packaging Materials*; TAPPI: Atlanta, GA, USA, 2022.
43. TAPPI. *T 559 cm-12 Grease Resistance Test for Paper and Paperboard*; TAPPI: Atlanta, GA, USA, 2012.
44. *ASTM E96/E96M-16*; Standard Test Methods for Water Vapor Transmission of Materials. ASTM: West Conshohocken, PA, USA, 2016.
45. *ASTM D3985-17*; Standard Test Method for Oxygen Gas Transmission Rate Through Plastic Film and Sheeting Using a Coulometric Sensor. ASTM: West Conshohocken, PA, USA, 2017.
46. TAPPI. *Air Resistance of Paper (Gurley Method) T460*; TAPPI: Atlanta, GA, USA, 2002.
47. Schneider, C.A.; Rasband, W.S.; Eliceiri, K.W. NIH Image to ImageJ: 25 years of image analysis; Brief Communication. *Nat. Methods* **2012**, *9*, 671–675. [CrossRef]
48. TAPPI. *Viscosity of Pulp (Capillary Viscometer Method)*; TAPPI: Atlanta, GA, USA, 2023.

49. Smith, D.K.; Bampton, R.F.; Alexander, W.J. Use of New Solvents for Evaluating Chemical Cellulose for the Viscose Process. *Ind. Eng. Chem. Process Des. Dev.* **1963**, *2*, 57–62. [CrossRef]

50. Li, A.; Xu, D.; Luo, L.; Zhou, Y.; Yan, W.; Leng, X.; Dai, D.; Zhou, Y.; Ahmad, H.; Rao, J. Overview of nanocellulose as additives in paper processing and paper products. *Nanotechnol. Rev.* **2021**, *10*, 264–281. [CrossRef]

51. Azeredo, H.M.C.; Rosa, M.F.; Mattoso, L.H.C. Nanocellulose in bio-based food packaging applications. *Ind. Crops Prod.* **2017**, *97*, 664–671. [CrossRef]

52. Ferrer, A.; Pal, L.; Hubbe, M. Nanocellulose in packaging: Advances in barrier layer technologies. *Ind. Crops Prod.* **2017**, *95*, 574–582. [CrossRef]

53. Moon, R.J.; Martini, A.; Nairn, J.; Simonsen, J.; Youngblood, J. Cellulose nanomaterials review: Structure, properties and nanocomposites. *Chem. Soc. Rev.* **2011**, *40*, 3941–3994. [CrossRef] [PubMed]

54. Wei, L.; Agarwal, U.P.; Hirth, K.C.; Matuana, L.M.; Sabo, R.C.; Stark, N.M. Chemical modification of nanocellulose with canola oil fatty acid methyl ester. *Carbohydr. Polym.* **2017**, *169*, 108–116. [CrossRef]

55. Saito, T.; Hirota, M.; Tamura, N.; Kimura, S.; Fukuzumi, H.; Heux, L.; Isogai, A. Individualization of Nano-Sized Plant Cellulose Fibrils by Direct Surface Carboxylation Using TEMPO Catalyst under Neutral Conditions. *Biomacromolecules* **2009**, *10*, 1992–1996. [CrossRef]

56. Franke, D.J.; Sabo, R.C.; Schilling, C.A. Durability of cellulose nanofibril films examined via residual drying stress measurement. *Cellulose* **2024**, *31*, 10845–10859. [CrossRef]

57. Mazega, A.; Tarrés, Q.; Aguado, R.; Pèlach, M.À.; Mutjé, P.; Ferreira, P.J.T.; Delgado-Aguilar, M. Improving the barrier properties of paper to moisture, air, and grease with nanocellulose-based coating suspensions. *Nanomaterials* **2022**, *12*, 3675. [CrossRef]

58. Shojaeiarani, J.; Bajwa, D.; Holt, G. Sonication amplitude and processing time influence the cellulose nanocrystals morphology and dispersion. *Nanocomposites* **2020**, *6*, 41–46. [CrossRef]

59. Gicquel, E.; Bras, J.; Rey, C.; Putaux, J.-L.; Pignon, F.; Jean, B.; Martin, C. Impact of sonication on the rheological and colloidal properties of highly concentrated cellulose nanocrystal suspensions. *Cellulose* **2019**, *26*, 7619–7634. [CrossRef]

60. Girard, M.; Bertrand, F.; Tavares, J.R.; Heuzey, M.-C. Rheological insights on the evolution of sonicated cellulose nanocrystal dispersions. *Ultrason. Sonochem.* **2021**, *78*, 105747. [CrossRef] [PubMed]

61. Beck, S.; Bouchard, J.; Berry, R. Controlling the reflection wavelength of iridescent solid films of nanocrystalline cellulose. *Biomacromolecules* **2010**, *12*, 167–172. [CrossRef] [PubMed]

62. Nechyporchuk, O.; Belgacem, M.N.; Pignon, F. Current progress in rheology of cellulose nanofibril suspensions. *Biomacromolecules* **2016**, *17*, 2311–2320. [CrossRef]

63. Ilyas, R.A.; Azmi, A.; Nurazzi, N.M.; Atiqah, A.; Atikah, M.S.N.; Ibrahim, R.; Norrrahim, M.N.F.; Asyraf, M.R.M.; Sharma, S.; Punia, S. Oxygen permeability properties of nanocellulose reinforced biopolymer nanocomposites. *Mater. Today Proc.* **2022**, *52*, 2414–2419. [CrossRef]

64. Martínez-Sanz, M.; Lopez-Rubio, A.; Lagaron, J.M. High-barrier coated bacterial cellulose nanowhiskers films with reduced moisture sensitivity. *Carbohydr. Polym.* **2013**, *98*, 1072–1082. [CrossRef]